UNIVERSITY OF OKLAHOMA

GRADUATE COLLEGE

EXPERIMENTAL ANALYSIS OF CENTRIFUGAL DOWNHOLE SEPARATORS IN BOOSTING ARTIFICIAL LIFT PERFORMANCE

A THESIS

SUBMITTED TO THE GRADUATE FACULTY

in partial fulfillment of the requirements for the

Degree of

MASTER OF SCIENCE

By

MICHAEL OLAYEMI OLUBODE

Norman, Oklahoma

2021

EXPERIMENTAL ANALYSIS OF CENTRIFUGAL DOWNHOLE SEPARATORS IN BOOSTING ARTIFICIAL LIFT PERFORMANCE

A THESIS APPROVED FOR THE

MEWBOURNE SCHOOL OF PETROLEUM AND GEOLOGICAL ENGINEERING

BY THE COMMITTEE CONSISTING OF

Dr. Hamidreza Karami, Chair

Dr. Xingru Wu

Dr. Pejman Kazempoor

Acknowledgements

I applied to the University of Oklahoma because of Dr. Hamidreza Karami's rich profile in Production Engineering. I appreciate his expertise and grace in his course delivery, and I am excited that I got to work with him. I haven't worked with a humbler and more gracious professor than Dr. Karami. I am grateful for the liberty I had under him to try and figure things out, and he was always available to give guidance and correction to my work.

Thanks to Dr. Xingru Wu, your Well Testing course is one of the best classes I have taken at OU petroleum engineering. I appreciate your guidance and evaluation of this study. I also appreciate Dr. Pejman Kazempoor for contributing his knowledge of Mechanical Engineering into evaluating this work, it has only improved the quality of this work.

Special thanks to Jeff McCaskill for his support in equipment installation and replacement. Our workshop surely runs on your technical support. I also enjoyed working with amazing research partners, I appreciate the supports of Platin Iradukunda, Eduardo Cerqueira and Laura Osorio in running the numerous experiments. I also appreciate Ashutosh Sharma for sharing his experience on the study. Ryan Bodlak and Emmanuel Alagbe are also appreciated for their support in my drawings.

I appreciate the Nigerian community at OU and Oklahoma in general. Thanks to my friends at MPGE and Antioch community church for making me feel at home. I am grateful for you all. I also appreciate Temilade and Jenrola for their overseas moral support.

Finally, I appreciate the unconditional love and care of my siblings and mother. Glory to God for the success of this work.

Table of Contents

List of Tables

List of Figures

Abstract

Gas evolution and expansion is a natural phenomenon in oil and gas wells. However, gas is detrimental to pumping artificial lift (AL) systems, causing incomplete pump fillage and reduced pump efficiency in oil wells. Pumping AL systems may also be involved in high GLR applications for well deliquification. It then becomes essential to separate the gas before the pump's intake in these applications to preserve the life of the pump. Various downhole separators with questionable efficiencies are available today. In this study, an automated experimental separation facility is presented and applied to test the efficiency of a novel centrifugal separator. The setup includes a 31-ft horizontal section followed by a 27-ft vertical section that contains the centrifugal separator. The performance of the separator is evaluated at different air (34 - 215 Mscf/d) and water rates (17 - 867 bpd). The multiphase-flow loop is equipped with pressure transducers and control valves for effective flow control. Data acquisition and process control are performed using Labview^{TM}.

A newly designed packer-type centrifugal downhole separator is evaluated over a wide range of flowrates and compared to a basic gravity separator without the centrifugal part. The performance and outlet flow stability of the separators are compared. Liquid separation efficiency is a measure of the ratio of the inlet liquid produced at the tubing return line. Output flow stability is measured by looking at the ratio of standard deviation over the average flowrate. Separation efficiency is close to ideal (100%) for liquid rates up to 500 bpd for both separators. The efficiency slightly reduces at higher liquid rates but stays above 80%. This decline in efficiency is more noticeable for the gravity separator compared to the centrifugal one, and it is sharper for higher gas rates (over 300 SCF/STB). The centrifugal separator provides a more stable output flow rate with less fluctuations compared to the gravitational one. Various flow patterns in the separator

outlet and the casing are visualized and recorded.

With declining rates of production from oil fields and the need to deliquefy gas wells, efficient artificial lift is necessary. This system provides a unique and novel tool to simulate the dynamics of flow in wellbores and identify the best tools to improve this efficiency.

CHAPTER 1: INTRODUCTION

1.1 Problem Statement

The presence of gas in oil wells can be considered as both a blessing and a curse. This may include the free gas present in the reservoir, or the gas released from the live oil solution. Gas is released from the solution as the pressure drops along the production system. Pressure drops as the fluid travels up the tubing string releasing solution gas from the produced fluid. Another cause for pressure depletion in producing wells is the decline in reservoir pressure over time. This pressure drop may lead to in-situ liberation of gas in the reservoir, resulting in significant gas amounts at the well bottomhole. For most producing wells, the gas presence is so inevitable that it impacts operators' decisions for artificial lift techniques to use.

The expansion of brownfields has made effective and improved artificial lift methods necessary. In most circumstances, the pressure depletion that necessitates artificial lift can also drive the produced fluid into the two-phase region of the phase envelope. This process of decline in reservoir pressure is shown for a representative phase envelope in Figure 1.1, pushing the fluid production into the two-phase region.

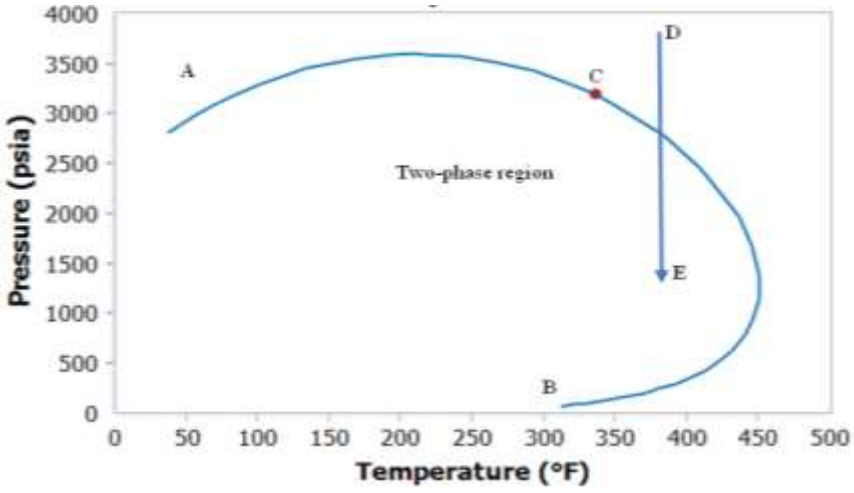

Figure 1.1. Phase Envelope of a volatile oil

While gas-lift is enhanced by the presence of gas, gas is detrimental to pumping artificial lift methods. Figure 1.2 shows the market share of different artificial lift methods in the U.S. from 2014 to 2025. The available historical data used in the chart is from 2014 to 2016 while the following years are predicted.

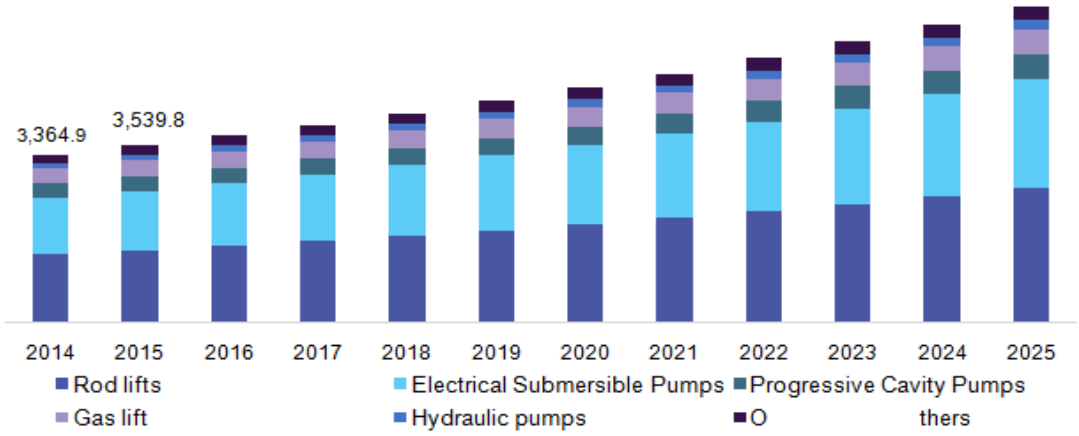

Figure 1.2. U.S. artificial lift systems market by product. (USD Million). Source: Grand View Research

From the presented data in Figure 1.2, pumps dominate the artificial lift use. Hence, it is important to evaluate the effects of gas on pumps and mitigate them. When gas is present in the chamber of a rod pump during the downstroke, the traveling valve moves some distance and compresses the gas before the pressure builds up enough to open the valve. This behavior causes gas lock and fluid pound, which are detrimental to pumps.

Operators are interested in driving down production costs by reducing damage to equipment and minimizing downtime for equipment repair or replacement. Gas interference causes reduced pump efficiency, production heading, and intermittent production. It is important for operators to efficiently manage gas downhole. This necessitates the use of downhole separators.

Downhole separators are placed upstream of the pump as a solution to the problem of gas interference. Downhole separators separate gas from liquid, ensuring that most of the liquid goes

into the pump through the tubing, while the gas is produced through the casing-tubing annulus. This reduces gas interference in pumps, allowing for better productivity and longer pump life. If operators cannot separate the gas downhole, they are forced to use less efficient methods like hydraulic pumps or gas lift instead of electric submersible pumps (ESPs), which can deliver higher flowrates (Kobylinski et al., 1985). Gas separators enable operators to use ESPs with higher GORs than would otherwise be considered possible (Kobylinski et al., 1985). This study aims to evaluate the performances of various downhole separator types.

1.2 Objective

This study has the following main objectives:

- Quantitatively evaluate the separation efficiency of two packer-type downhole separators, a centrifugal and a non-centrifugal one.
- Analyze the effects of liquid and gas rate operating conditions on separation efficiency and production stability, identify the ranges of optimum separator performance.
- Compare the performances of the two downhole separators to understand the impact of centrifugal forces on downhole separation efficiency.
- Identify the effect of inlet flow dynamics on separation efficiency and production stability.

1.3 Scope of Work

The nature of this work is experimental. The facility was designed to test varying inlet gas and liquid rates and analyze the effects of the changes at the outlet. This was followed by data collection at designed liquid and gas rates making up the test matrix. There are two stages of experiments presented in this study, first using the centrifugal separator, and then with the non-centrifugal gravity separator. Both testing stages are conducted over an extended range of liquid

and gas flow conditions. The effects of both separator geometry and flow conditions are tested on separation efficiency.

This work includes five chapters. First, in Chapter 2, a review of the historical designs of downhole separators, their respective methods of separation and efficiencies is shown. Chapter 3 is the description of the experimental setup used for collecting data on the separators. Chapter 4 presents the analysis of the results. The performances of the separators are evaluated under varying operating conditions. Chapter 5 concludes on the key findings of this research, and provides some recommendations for the future work in this field.

CHAPTER 2: LITERATURE REVIEW

Gas separation technologies have been studied as early as 1963 when Clegg set some of the rules of thumb used in downhole gas separation (J. N. McCoy et al., 2005). It is established in literature that gas bubbles of 0.25 in. diameter will rise in water at a velocity of 6 in./s (Lopez et al., 2019). From Stoke's law, bubble rise velocity is proportional to bubble diameter which means gas bubbles greater than 0.25 in. diameter will flow upwards at a velocity higher than 6 in./s. Hence, downward liquid velocity of 6 in./s or less will allow gas bubbles of 0.25 inches in diameter and higher to separate. (Lopez et al., 2019) questioned this rule of thumb because good separation efficiency was obtained in their study even at liquid downward velocity greater than 6 in./s. A second condition needed for effective gas separation is that friction loses in the dip tube should be less than 1/2 psi to prevent gas breakout within the separator (J. N. McCoy et al., 1998). As a result, efforts at optimizing separator performance have been focused on maximizing the downward flow area or minimizing the annular liquid flow to achieve liquid velocities below 6 in./s (Kobylinski et al., 1985). This method allows gas to slip out of the liquid phase.

There are several types of downhole separators, also known as gas anchors, performing the function of in-situ separation of gas and liquid. The oldest and most efficient type of downhole separators is the natural gas separator (J N Mccoy et al., 2013). It requires no special equipment but to place the pump inlet below the perforation depth to allow formation fluids separate by gravity. In this completion, the casing-tubing annulus serves as the separator and provides the retention needed for gas to separate from the liquid which flows downward to the pump inlet. More information on the working technique and optimum depth below perforations is provided by (J.

M. McCoy et al., 2007). However, it is impossible to place the pump inlet below the perforation depth in most completions due to rathole restrictions or the possibility of sanding the pump (J. M. McCoy et al., 2007). Hence, the use of the natural-gas separator is limited despite its high performance. The limitations of the natural-gas separator give rise to another type of downhole separators which are used when pumps are placed above the formation fluid entry point. In addition to the natural-gas separator, there is the poor boy separator, modified poor boy separators (collar size), packer type separators and the special separators as given by McCoy.

Downhole gas separators are often the most inefficient part of a sucker rod pump system (J. M. McCoy et al., 2007) and this is due to the ease of making a downhole separator. A poor-boy separator is manufactured from a short joint of tubing string with perforations for venting gas. This leaves room for a major deficiency in separation performance because the tubing has limited area available for gas separation (J. M. McCoy et al., 2007).

Studies by (J. M. McCoy et al., 2007; J. N. McCoy et al., 2005; James N Mccoy et al., 2017) evaluated the effect of additional factors such as the length and diameter of the dip tube, and entry ports geometry and location on separator efficiency. These studies showed that the diameter of the dip tube affects separation efficiency due to the associated pressure drop. When the diameter is too small, frictional pressure loss increases, while gravitational pressure drops increases when the dip tube is too large and completely full of liquid. Both the Echometer type and Patterson gas separators exhibited the same behavior when dip tube diameter was varied. The effects of the entry ports were also investigated, and it was discovered that increasing entry ports diameter increases the flow of both gas and liquid into the separator. Gas and liquid are only drawn into the separator during pump upstroke in a conventional separator but the entry ports modification by McCoy allow fluid entry into the separator at both upstroke and downstroke cycles of the pump (McCoy et al.

1998). Another improvement employed by McCoy in the conventional downhole separator is to increase the area inside the downhole separator. Since poor boy separator is cut out of a tubing string, its diameter is less than the diameter of the collar. McCoy presented an improved separator with an O.D. equal to the collar O.D. and with an additional advantage of preventing sand fill around the bottom of the collar when separator and collar diameters are different. The improved separator, with enlarged outer barrel and thin wall for maximum area, is the modified poor boy separator. McCoy et al. made no conclusion on the effect of operating conditions on separation efficiency (Lopez et al., 2019).

Due to gravity, gas flows into the pump inlet when the pump is set above the perforation depth. A poor boy separator is used in packerless completions, when the pump intake is set above the perforation depth. A poor boy separator contains a chamber with perforated subs to vent gas before making it to the pump inlet. The use of a secondary chamber besides the casing-tubing annulus reduces the liquid capacity that the well can deliver to the pump (not to be confused with formation deliverability which depends on inflow performance relations). Separator liquid capacity is the maximum liquid rate that does not entrain gas into the pump (James N Mccoy et al., 2017).

Packer-type separators use the technique of the natural-gas separators while considering the rathole restrictions that prevent setting the pump intake below the perforation depth. In a clearer sense, this separator type is located above the perforation depth and the end of tubing packer and simulates the natural-gas separation (J. N. McCoy et al., 2015). Once the inlet fluid passes through the packer, it is diverted to the separator attached to the tubing. The separator reduces the kinetic energy of the fluid, separates the fluids by gravity, and sends the gas to the annulus above the packer. (Lopez et al., 2019) analyzed the performance of an inverted shroud separator under

varying operational conditions, deviation angles and flow pattern upstream of the separator. The effect of different separation techniques on separation efficiency was not evaluated in their study. (J. N. McCoy et al., 2015) performed field testing of 27 wells consisting of 14 completions with natural-gas separators and 13 wells with packer-type separators. The results showed an average pump liquid fillage of 86% for the natural gas separators and 62% for the packer-type separators. The lower efficiency of the packer-type separators was attributed to the lack of design optimization for pressure drop in the separator. (J. N. McCoy et al., 2013) presented several ways of optimizing packer-type separators by adding additional parts like check valve, tail pipe or replacing the packer with a diverter cup. None of the optimization introduced additional separation technique other than gravity in the separator.

Most of the gas anchors work on gravity (Sharma et al., 2020). However, the effect of centrifugal force on downhole gas separation has also been explored (Kobylinski et al., 1985, Bohorquez et al., 2009) to a lesser extent. A centrifugal separator achieves separation of gas and liquid using cyclone and vortex technology. Centrifugal separators combine agitation and the centrifugal effect to optimize separation. Separated liquid is led to the wall as it is thrown tangentially, while the gas stays at the center of the tubular. A centrifugal separator is an active-type device, and it can separate the gas at liquid rates as high as 8000 B/D (Kobylinski et al., 1985).

This study is a continuation of the work done by (Sharma et al., 2020) where a centrifugal separator was investigated for gas and liquid separation efficiency. Sharma concluded that liquid and gas separation efficiency values increase with increasing flowrate. However, more tests were run in this study, revealing that efficiency only increases until a certain threshold before it begins to decrease. The performance of a centrifugal separator is analyzed over an extended range of flowrates. The separator's performance is compared with that of a basic gravity type separator.

CHAPTER 3: FACILITY AND EXPERIMENT DESIGN

The multiphase flow facility used in this study is located at the Well Construction Technology Center (WCTC) of the University of Oklahoma. The schematic of the facility is shown in Figure 3. 1. It consists of 5 sections covering the entry of fluid mixture into the system, separation into constituent phases at the separator, and eventual exits and metering at the casing and tubing return lines. All parts of the facility and their contributions to the performance of the experiments are discussed in this chapter.

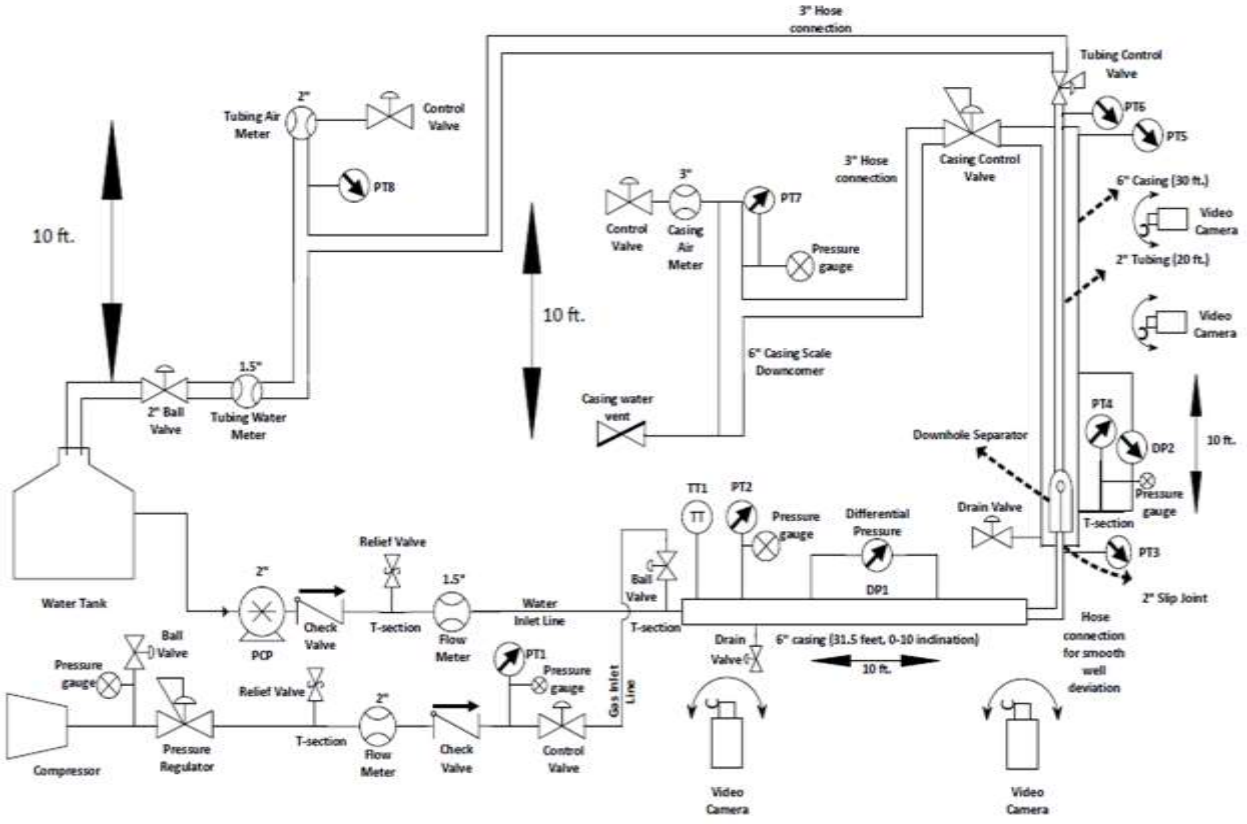

Figure 3. 1. Multiphase flow facility schematic (Sharma, 2019)

3.1. Detailed Facility Design

The facility is divided into 6 distinct segments. These segments are listed below:

1. Gas inlet line (GIL)
2. Water inlet line (WIL)
3. Horizontal section
4. Vertical section
5. Tubing return line (TRL)
6. Casing return line (CRL)

3.1.1. Gas inlet line (GIL)

Gas enters the facility via the gas inlet line. It is delivered from a rotary screw compressor (Figure 3.2) with maximum capacity of 1600 scfm. A control valve downstream of the flowmeter is actuated by voltage output from the data acquisition (DAQ) card, discussed later in this chapter. This control valve is used to set the required gas flowrate for each experiment.

Figure 3.2. Compressor

Figure 3.3 is a schematic of the GIL from the compressor to the mixing T, where water and air are mixed. The compressor is connected to the facility through a flexible hose and metal nipple. The pressure gauge between the compressor and the pressure regulator in Figure 3.3 is used for

monitoring pressure level in the gas line. Next to the pressure gauge is a ball valve that serves to bleed the trapped pressure when the compressor is turned off. Bleeding the gas line at the end of the day is a safety measure observed after the compressor is powered off and before disconnecting the flexible hose from the compressor.

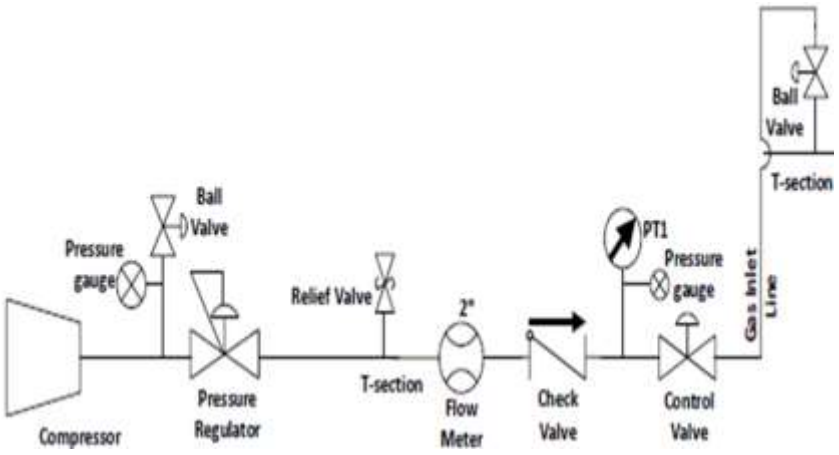

Figure 3.3. Gas inlet line schematic

The pressure rating of the compressor is higher than the maximum pressure needed for the experiments. Hence, a pressure regulator is used to maintain the desired pressure in the lines. The pressure regulator is of size 1.5-in., with maximum pressure and temperature of 300 psig and 160 ^{o}F, respectively. It was used to limit the pressure downstream of it to 30-40 psig for the tests of this study. The relief valve before the 2-in. Coriolis flowmeter is set to pop open when the pressure is greater than 100 psig. This valve is faced downward to keep people and equipment away from the pressure path should the valve pop open.

Inlet gas flowrate is measured by Coriolis meter at the GIL, the flowmeter is labeled FM-1. Coriolis meters are reputed for their accurate measurement of gas flowrates. Motion mechanics lies at the heart of a Coriolis flow meter's operation (Sharma, 2019). Fluid is allowed to pass through a vibrating tube, which accelerates it as it approaches peak amplitude vibration. The oscillation of the tubes generates voltage from each peak during operation, resulting in a sine wave.

The mass flow rate is directly proportional to the measured time delay between two sine waves, whereas the amplitude of the waves is a measure of fluid density. The DAQ card, which is attached to the computer, is wired to all of these equipment. The flowmeter is used to obtain the mass flowrate, temperature, and density of the inlet gas.

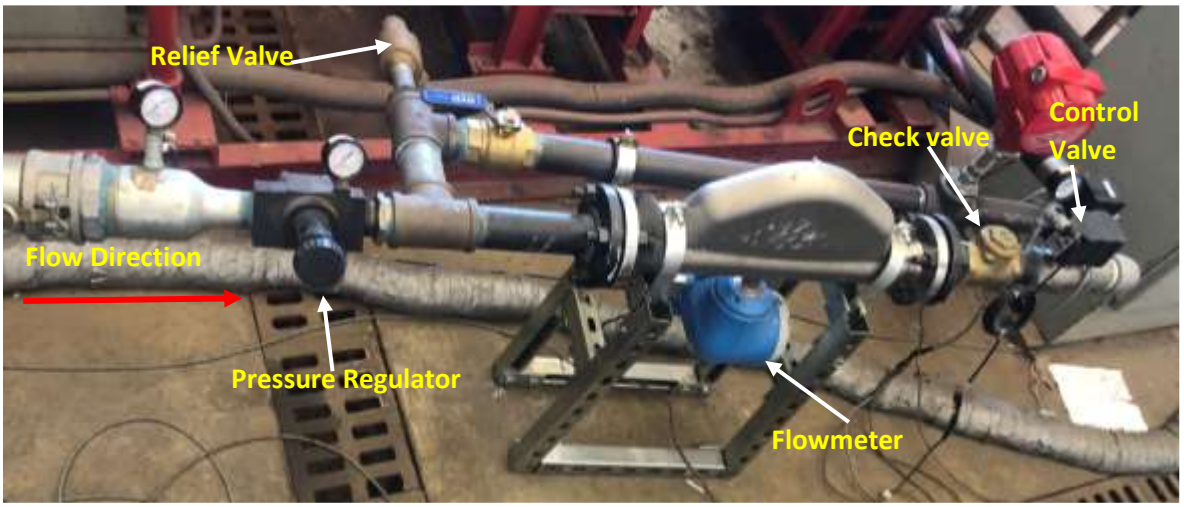

Figure 3.4. Gas inlet line photograph

The next equipment in the GIL is the check valve, which prevents backflow of gas in the line. It ensures gas does not flow back into the flowmeter. PT1 and control valve are connected to the DAQ card. The actuator of the control valve ranges between 0-10 volts, which represents 0-100% opening of the control valve. If a 5-volts signal is sent from the DAQ card to the control valve, it implies a 50% opening of the control valve. The opening of the control valve regulates the gas inlet flowrate. The control valve is then connected through a flexible hose to the T-section, where GIL mixes with the water inlet line.

3.1.2. Water inlet line (WIL)

The schematic of the water inlet line is shown in Figure 3.5. It consists of the water tank, pump, valves, flowmeter, and ends at the mixing T-section. The water tank has a capacity of 150 gallons. Since the facility is a closed-loop system, this is a sufficient volume to keep the

experiments running for long times. The tank is connected to a progressing cavity pump (PCP) through a 2-in. flexible hose and a nipple. The PCP is rated at 60 gpm maximum flowrate, although the highest water flowrate tested for this study was 26 gpm.

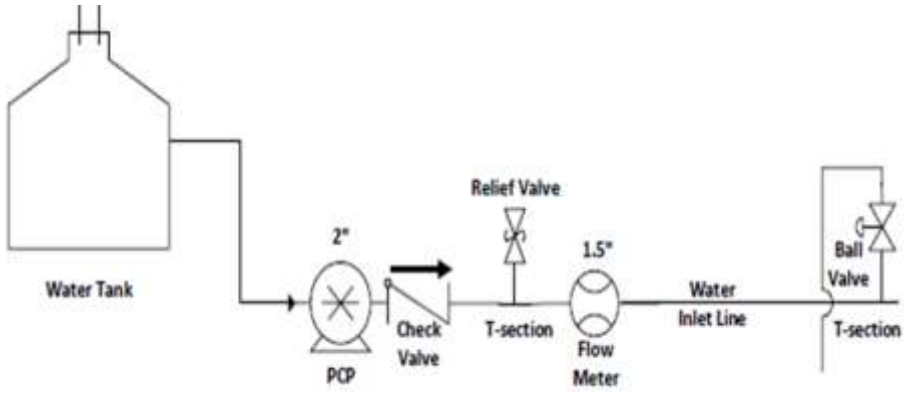

Figure 3.5. Schematic of the water inlet line (WIL) (Sharma, 2019)

The pump is controlled from the data acquisition system through a variable speed drive (VFD), as shown in Figure 3.6. VFD is an output device receiving voltage from the DAQ system. It is used to control the speed of the PCP, which in turn determines the flowrate delivered by the pump. The required PCP speed corresponding to a water flowrate is determined through a PID controlling scheme. The water flowrate measured at the flowmeter is used for this purpose. In the PID control, a target flowrate is set on the control application developed on LabVIEW^{TM}. The PID controller then changes the speed of the PCP until the desired flowrate is obtained at the flowmeter. The PID control was eventually replaced by a simple equation relating the voltage delivered and the water flowrate.

Figure 3.6. Water inlet line

The flowmeter at the water inlet line is a Coriolis flowmeter labeled FM-2, with a general working principle of estimating flowrates through a vibrating tube. FM-2 measures the mass flowrate, density and temperature of the liquid flowing through it. A 2-in flexible hose with 150 psig pressure rating is then used to connect the flowmeter to the T-section, where water mixes with air. The mixture then enters the horizontal section.

3.1.3. Horizontal section

The schematic of the horizontal section is shown in Figure 3. 7. The horizontal section consists of a 3-in. metal nipple, a 3 to 6-in. metal bushing, a 6-in. PVC collar, three joints of 6-in. PVC pipes, a high strength aluminum frame stand, metal and straub clamps, a 6 to 2-in. PVC bushing, a 2-in metal nipple, a hose pipe to connect the horizontal and vertical sections, and a differential pressure transducer (Sharma, 2019). Gas and liquid mix at a T-section and enter the horizontal section of the facility, which simulates flow in a horizontal well. A check valve prevents

back flow of liquid from the mixing T-section into the gas line. The horizontal flow section is made of 31-ft of 6-in. ID PVC pipe. The flow of the gas and liquid mixture is turbulent near the inlet mixing T-section. However, there is a separated flow pattern downstream of the T-section. The liquid-gas mixture then enters the vertical section through a flexible riser, where the change of elevation mixes the fluids again. The fluids enter the vertical section through a 2-in. PVC pipe that leads to the separator.

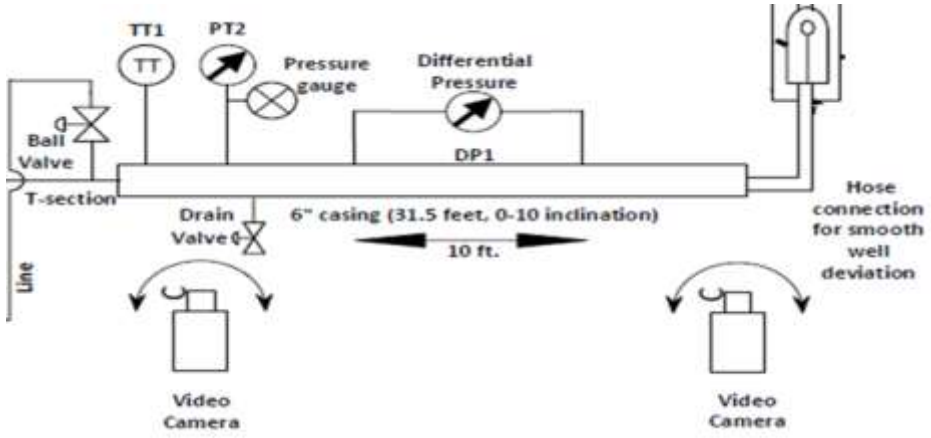

Figure 3. 7 Schematic of horizontal section

3.1.4. Vertical Section

The schematic of the vertical section is provided in Figure 3.8, with a lengthier description in Sharma (2019). A pressure transducer, PT-3, at the entrance of the vertical section, measures the pressure of the inlet mixture. The next equipment is the downhole separator which opens to the casing annulus. A pressure transducer, PT-4, placed in the casing annulus below the separator's level and a differential pressure (DP) cell measure the pressure drop across the separator. Two downhole separators were tested for this study, a centrifugal and a gravitational one. They will be described in more details later. The vertical section simulates a vertical wellbore with a packer, production tubing, and a downhole separator installed above the packer's level.

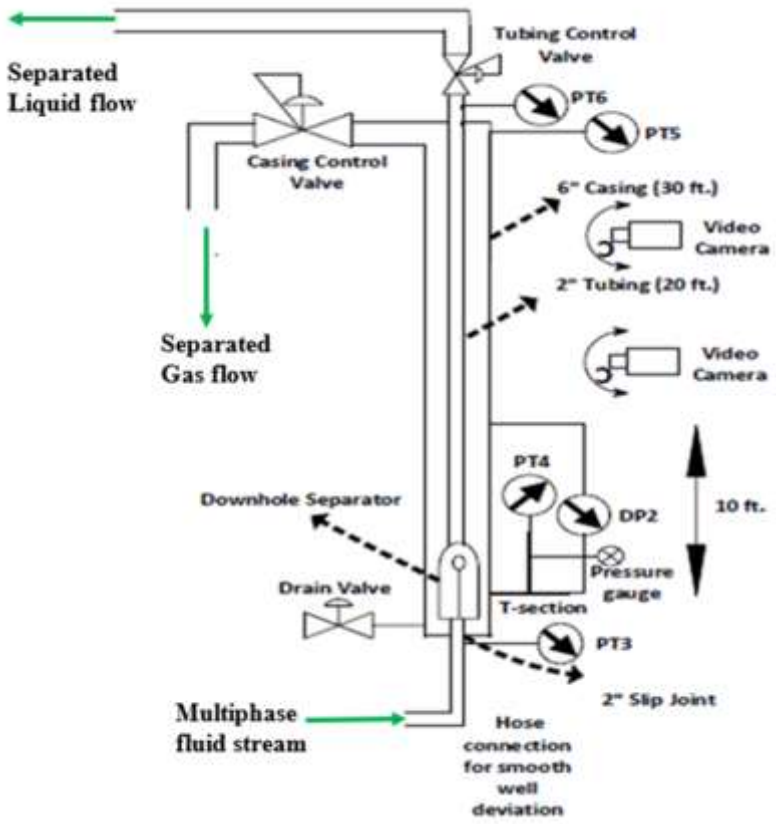

Figure 3.8. Schematic of the vertical section

Video footage of the flow pattern is taken at two locations along the vertical section. One camera is at the outlet of the spiral section of the separator to observe the flow characteristics of the mixture as it exits the separator and the liquid falls in the annulus. The second camera is at the shroud inlet to visually analyze the size and speed of the gas bubbles entering the tubing.

The wellhead contains two pressure transducers, PT-5 at the casing head and PT-6 at the tubing head, the casing control valve (CCV), and the tubing control valve (TCV). TCV was completely open for all the experiments of this study. The CCV was used to control liquid level in the annulus. The control mechanism used on the CCV is discussed in the next section.

3.1.5. Facility Control

The casing control valve (CCV) opening is an important part of the casing liquid-level control mechanism used in the facility. Depending on the liquid level in the casing, the CCV opening is adjusted to either choke the casing and push the liquid level down by gas pressure or to allow more gas to leave the annulus. The more the CCV opens, the lower the casing head pressure (PT-5) becomes; hence, liquid level rises in the annulus. In contrast, if the CCV opening reduces, the casing head pressure increases and creates a backpressure that lowers the liquid level in the annulus. The liquid level control is necessary for two reasons:

1. To prevent the gas from entering the shroud and tubing (a condition that results in incomplete pump fillage in actual field installations), and
2. To prevent liquid production from the casing.

The CCV is a pneumatic valve, which is electrically actuated by sending the corresponding voltage to it from the DAQ system. Proportional Integral Derivative (PID) control mechanism is used to adjust the liquid level in the annulus. The set-point of the PID controller is the difference between PT-5 (casing head pressure) and PT-6 (tubing head pressure). Figure 3.8 shows the locations of these pressure sensors. The process variable is the CCV opening. The PID control facilitates separation by adjusting the gas flow through the control valve. It reduces liquid carryover in high gas velocities and limits gas carry-under into the tubing in high liquid velocities. Considering the casing-tubing system as a U-tube, a target pressure difference of 6.3 psi between casing and tubing heads is used. This pressure difference sets the liquid level just above the separator outlet in casing with tubing full of liquid. This target difference (TD) is shown in Figure 3. 9 on LabVIEW^{TM}, the data acquisition and control software. A TD range of 5.5-7.5 psi was used

in the experiments to analyze the effects of liquid level in casing on separation efficiency. PID control is necessary to evaluate the separator's efficiency at steady state conditions.

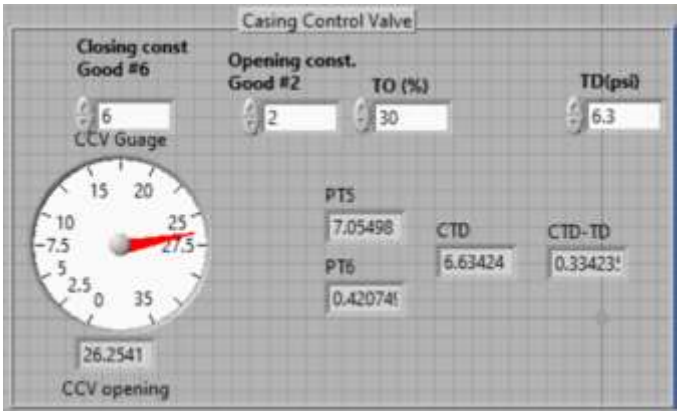

Figure 3. 9. LabVIEW interface of casing control PID scheme

3.1.6. Downhole separators

Figure 3.10(a) and Figure 3.10(b) show the schematic of the prototype centrifugal downhole separator from Echometer company. Gas-liquid mixture enters the separator from the tubing at point 88, Figure 3.10(a), flowing into the red and green ports in Figure 3.10(b) and passing through the spiral section 70. The spiral section imparts centrifugal force as it sends the mixture out of the separator. The liquid droplets impinge on the casing wall above the spiral. The impingement creates a loss in kinetic energy, allowing the liquid to fall and separate by gravity. Compared to other types of separators, separation is provided at two points, within the spiral section and in the casing above the spiral. Most of the gas separates at the spiral outlet and flows up to the casing head, while the liquid falls carrying some gas bubbles with it. The falling liquid eventually enters the shroud at point 102 and finds its way to the tubing at segment 24 in Figure 3.10(a), corresponding to the yellow ports in Figure 3.10(b). These entrance ports lead to the upper part of the tubing, downstream of the separator. The fluid leaving the separator is mostly liquid and is sent to the pump and produced at the wellhead.

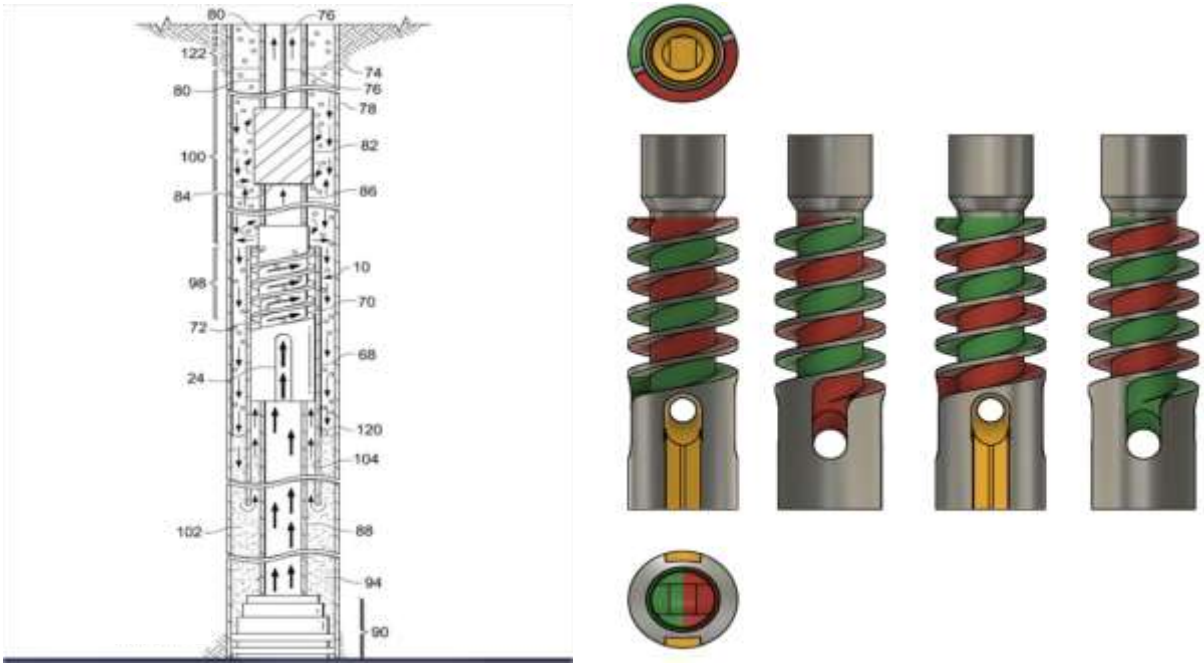

Figure 3.10. (a) Centrifugal separator within casing, (b) separator schematic

Figure 3.11 shows the schematic and photograph of the non-centrifugal-type separator. The geometry is similar to the centrifugal separator except for the lack of spiral section and the length, which is 10-in. compared to 15.5-in. for the centrifugal separator. The gravity separator was designed on Solidworks^{TM} using similar specifications to the centrifugal separator, and then printed on a 3D printer. The aim of the non-centrifugal separator is to compare the efficiency of the two separators so as to understand the effect of the spiral section on separation efficiency.

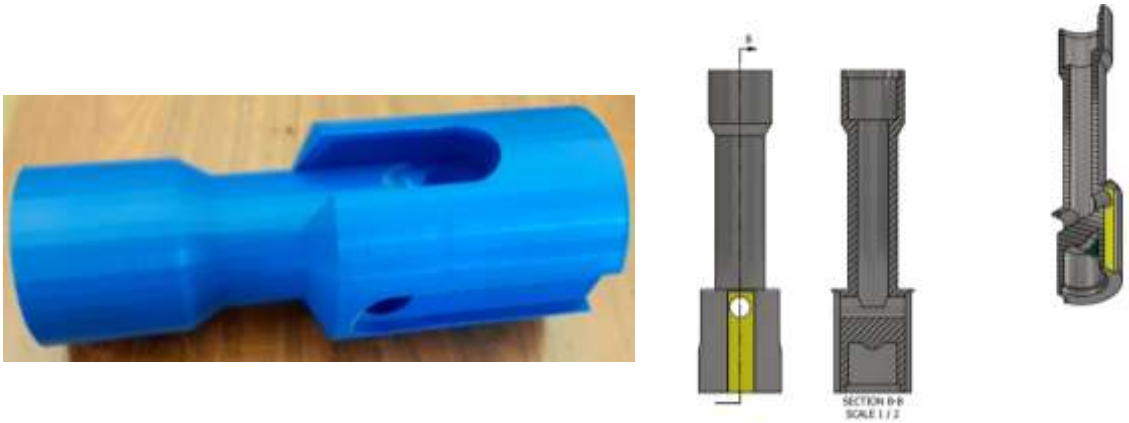

Figure 3.11. (a) Non-centrifugal separator photograph, (b) schematic

Figure 3.12 shows a simplified free body diagram of a liquid droplet and a gas bubble in the casing annulus. F1 is the centrifugal force pushing body to the casing wall while F2 is the opposing centripetal force pulling the body to the center of the flow. F4 is the gravitational force due to the density of the body and F3 is the buoyancy force dragging the body upwards.

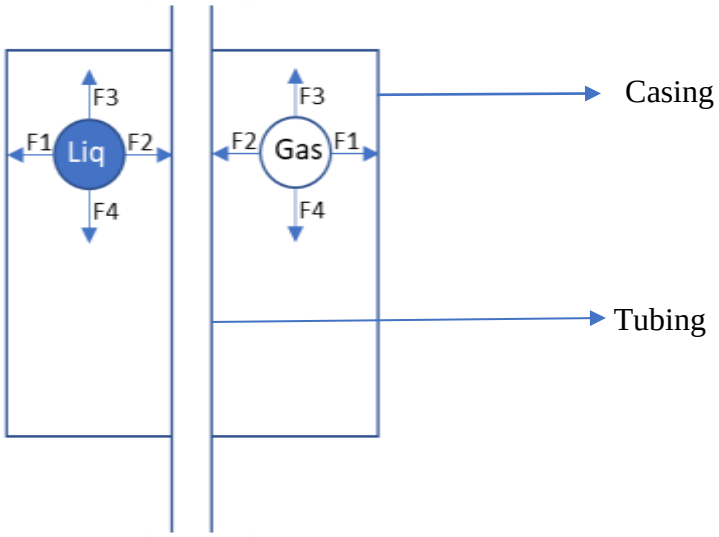

Figure 3.12. Free body diagram of gas bubbles and liquid droplets in casing annulus

All four forces act on the body in case of the centrifugal separator. F1 is greater than F2 for the liquid droplets, while F2 is greater than F1 for the gas bubbles. However, F1 and F2 are not present for the basic gravity separator, because the spiral part which imparts the centrifugal effect is missing. The governing forces in the basic gravity separator are only the upward and downward forces, earning the separator its name.

3.1.7. Tubing Return Line (TRL)

The tubing return line is a 10-ft long PVC pipe of 4-in. diameter placed parallel to the vertical section of the facility. It is divided into two segments of 5-ft each as seen in Figure 3.13. The TRL serves as a vertical separator to separate any trapped gas in the tubing production. A pressure transducer, PT-8, and a flowmeter (FM-4, $Q_{max} = 30\, lb/min$) are installed at the top of

the return line, where entrained air is metered and vented to the atmosphere. A 2-in. Coriolis gas flowmeter was initially installed at the TRL and used for the first set of experiments. However, since the expected gas flowrate at the TRL is less than 3 lb/min, the gas flowmeter has to detect small flowrates accurately. The 2-in. Coriolis gas flowmeter was not serving this purpose, detecting no gas flow for most of the experiments even when there was noticeable gas flow into the TRL. This necessitated the replacement of the flowmeter. It was later replaced with a 1-in. Sage™ thermal flowmeter ($Q_{max} = 3\ lb/min$) for better precision in the measurements.

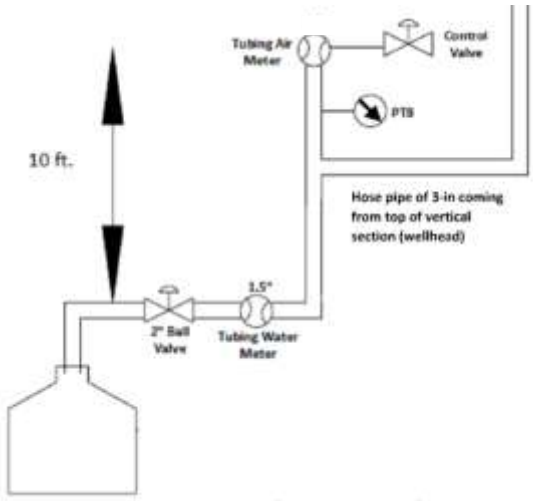

Figure 3.13. Schematic of tubing return line (TRL) (Sharma, 2019)

Above the flowmeter, the tubing control valve is installed to restrict gas flow in the TRL or to apply backpressure on the TRL, if needed. This valve was left open for all the tests performed at this study. The lower section of the TRL is connected to a 1.5-in. liquid flowmeter (FM-5) to measure the flowrate of the returning liquid. The liquid outlet of the TRL is connected to the water tank via a flexible hose to form a closed loop, as seen in Figure 3.14.

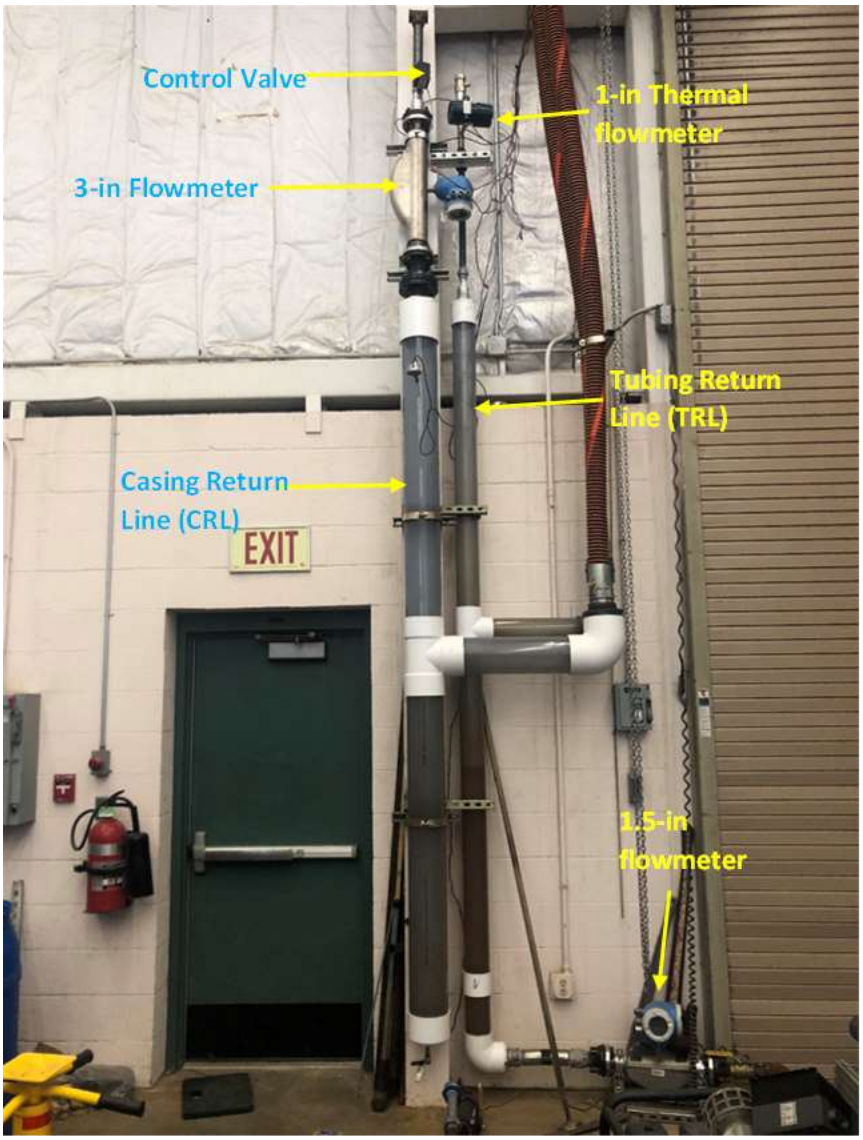

Figure 3.14. Photograph of the TRL and CRL

3.1.8. Casing Return Line (CRL)

The CRL, shown in Figure 3. 15, has the same geometry as the TRL except for the larger diameter of 6-in. It is installed in parallel to the TRL and acts as a vertical separator for the outlet stream of the casing, usually containing liquid slugs in early transients. It contains a pressure transducer, PT-7, and a 3-in. gas flowmeter for measuring outlet gas rate from the casing. The 3-in gas flowmeter ($Q_{max} = 100\, lb/min$) was later replaced with a 2-in gas flowmeter ($Q_{max} =$

30 lb/min) to improve the measurement accuracy and resolution. A control valve is installed after the casing air meter for the same purpose of introducing backpressure, if so desired. This control valve was left fully open for the tests of this study.

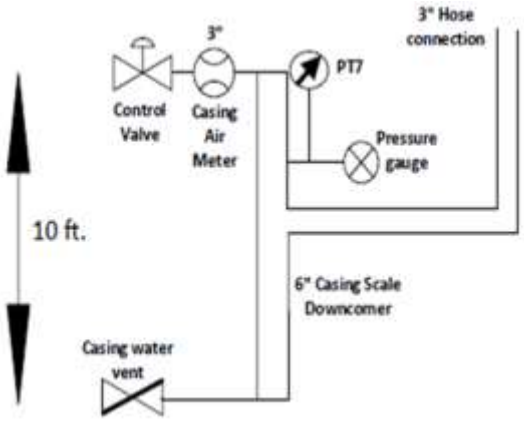

Figure 3. 15. Schematic of the casing return line

The gas rises to the top of the column and gets measured by the casing air meter (FM-3) before venting to the atmosphere. The liquid produced from the casing is not metered. It can be drained through a ¼-in. drain valve at the bottom of the column. This is because most of the liquid is produced from the tubing return line except for early transients at the beginning of each experiment. The drained liquid's volume can be measured to infer the separator's inefficiency. It takes an average of 5 minutes to attain steady state in the tests depending on gas and liquid rates.

3.2. Wiring and Instrumentation

The detailed description of the facility wiring can be found in Sharma (2019). Some changes were made to the original wiring of the facility during this study. The two existing Omega OMB-DAQ-3000 series DAQ cards were replaced with an OMB-DAQ-2416-4AO card (Figure 3. 16), an Omega card compatible with LabVIEW. An OMB-DAQ-2416-4AO card has 32 single ended ports/channels, accommodating all the sensors in the facility. Since the OMB-DAQ-2416-4AO card can be used in either differential mode (e.g., thermocouple connection) or single ended

mode, the channels are labelled from 0H to 15H, followed by 0L to 15L to represent channels 0 to 31 accordingly.

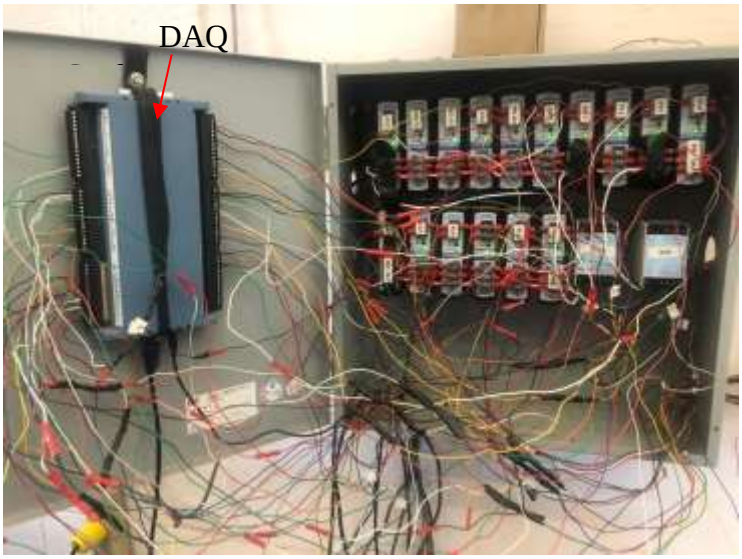

Figure 3. 16. Power box with DAQ card

The data acquisition card has four output ports, labelled VDAC0 to VDAC3, for sending voltage signals to the valves or the VFD. Current signals may also be sent by using a resistor with the voltage signal. A diagram for the data acquisition system connections is given in Figure 3. 17.

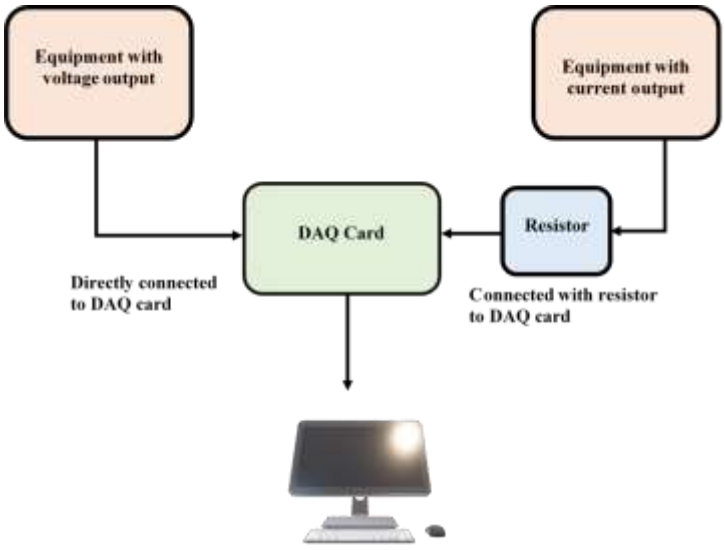

Figure 3. 17. Data acquisition system connection diagram (Sharma, 2019)

The four active output devices on the facility are the gas inlet line control valve, the casing control valve, the tubing control valve, and the water pump VFD. The casing control valve is a 6-in. pneumatic valve that takes current input from the DAQ card via a signal conditioner to amplify the transmitted signal sent to the pneumatic controller. The VFD is also connected to the DAQ card through a signal conditioner.

Table 3. 1 gives the inner port numbering and colors of the cables connected to the Coriolis flowmeters. Table 3. 2 shows the wiring details of all the input and output devices that are connected to the data acquisition card. LabVIEW channel order is the order in which the input devices are read into LabVIEW. This order is important in writing the data acquisition software used in logging the data and sending output signals to the control valves and the VFD.

Table 3. 1. Flowmeter port number and color coding

Coriolis Flow Meter		
Quantity	Port Number	Cable Color
Temperature	22	Yellow
	23	Brown
Density	24	Orange
	25	Green
Mass flowrate	26	Blue
	27	Red

Table 3. 2. Wiring details of sensors

LabVIEW Channel Order	Quantity	DAQ card Channel	Channel No.
1	PT-1	2L	18
2	PT-3	3H	3
3	PT-4	3L	19
4	PT-5	4H	4
5	PT-6	4L	20
6	Temp-FM1	6H	6
7	Temp-FM2	6L	22
8	Temp-FM3	12L	28
9	Temp-FM4	13L	29
10	Temp-FM5	9L	25
11	Den-FM1	5L	21
12	Den-FM2	7H	7
13	Den-FM3	14H	14
14	Den-FM4	12H	12
15	Den-FM5	9H	9
16	FM-2	7L	23
17	FM-5	8L	24
18	FM-1	5H	5
19	FM-3	13H	13
20	FM-4	14L	30
21	PT-7	11H	11
22	PT-8	11L	27
23	PT-2	15H	15
24	DP-1-Horiz	10H	10
25	DP-2-Vert	10L	26
26	TT-1	15L	31
0	VFD	VDAC0	N/A
1	CCV	VDAC1	N/A
2	TCV	VDAC2	N/A
3	GIL	VDAC3	N/A

Channel number can be inferred from the DAQ card channel. The H or L suffix of the channel represents high and low, when the DAQ card is used in differential mode. However, both H and L are used independently in single-ended mode. L channels are numbered after exhausting

the H channel numbers. This makes channel number 16 the first L channel (0L) and channel 31 the last one (15L).

3.2.1. LabVIEW Control Program

LabVIEW is the acronym for Laboratory Virtual Instrument Engineering Workbench. It is a systems engineering software for applications that require testing, measurement, and control with rapid access to hardware and data insights (National Instruments). LabVIEW offers a graphical programming interface that allow users to visualize and record all of their applications. The software is divided into two windows; the block diagram, where the graphical program is written/designed, and the front panel, where users interact with the written application.

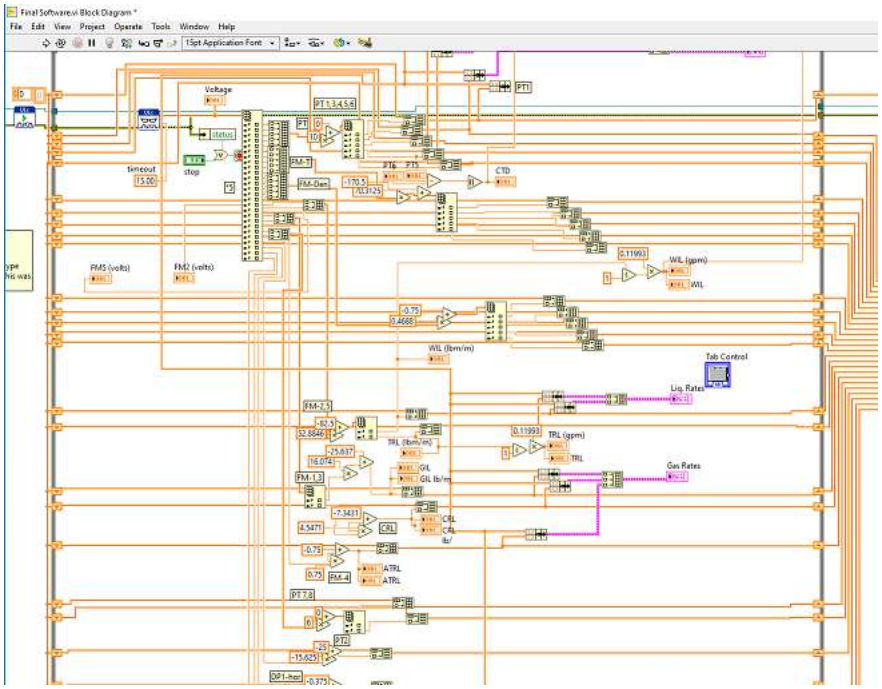

Figure 3. 18. LabVIEW Application block diagram

DAQ cards serve as an intermediate between equipment and the computer, in this case, between the sensors and valves, and the application developed on LabVIEW. A third-party virtual instrument (VI), called ULx, was used to allow the card to interact with the software. Figure 3. 19

is the front panel built on controls and indicators. Controls serve as input and allow the user to send information to the application, while indicators are used to display information to the users. At Figure 3. 19, GIL (%), TD (psi) and similar panels that are not greyed out are examples of controls. All of the gauges and plot area seen on the front panel are examples of indicators as they display the values of the associated quantities in real time.

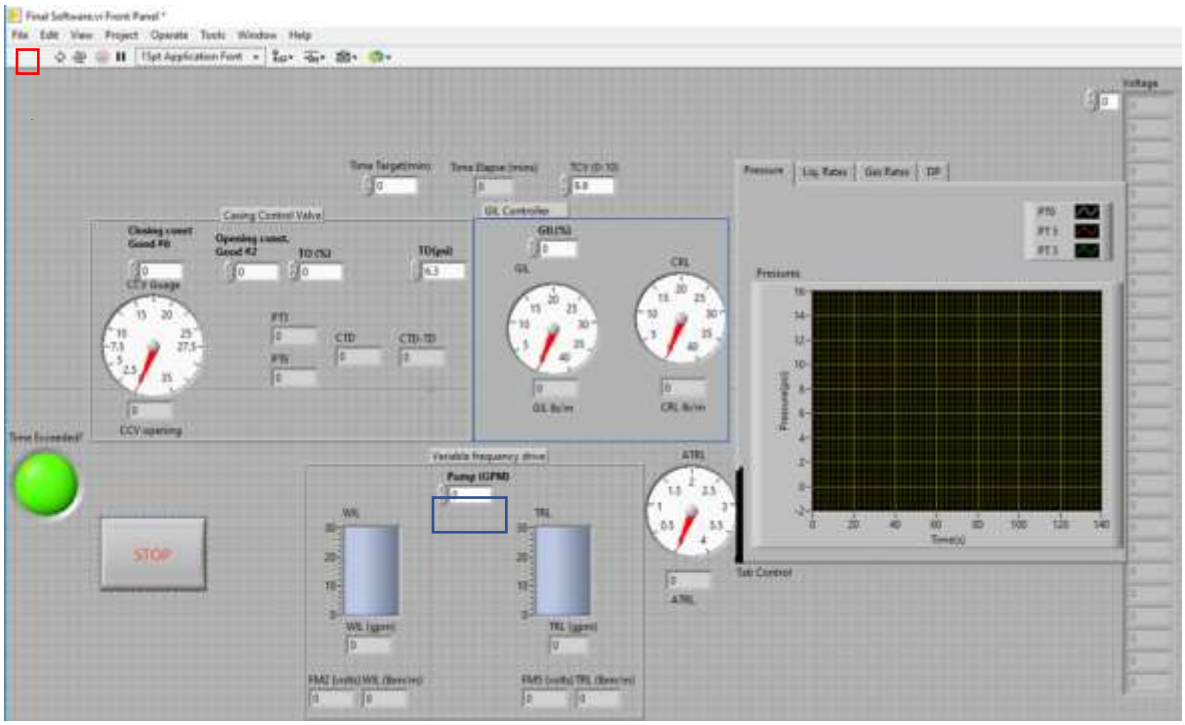

Figure 3. 19. LabVIEW Application front panel

Since LabVIEW has a graphical programming interface, applications can be developed by dragging and dropping objects representing the physical devices. This task is completed in the block diagram window, which is built on controls, indicators, structures, and functions. Each object on the front panel is also found in the block diagram as a terminal. An example is Pump (GPM) control in Figure 3. 19. The terminal on the block diagram is shown in Figure 3.20, where pump (GPM) is connected to the multiplication function to convert the pump rate input in gallons per minute from the user to voltage units sent to the VFD.

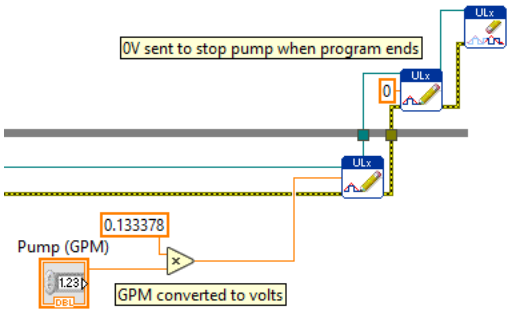

Figure 3.20. Pump terminal on block diagram

The application developed for this facility can be divided into three major parts, as seen in Figure 3.21. The first part includes the processes that occur just before the application starts running at the beginning of each experiment. In this section, all the input and output channels are opened, and each is assigned its upper and lower measurement limit. This is important to prevent accidental inputs from users that might damage an equipment. It is a good programming practice to not automatically trust user inputs. The 4 output channels are opened using separate write channel VI, but all of the 27 input channels are read on a single read VI. This is to reduce clutter of objects on the block diagram. This practice implies that the order in which channels are selected must be noted to prevent mismatch of calibration equations with sensors.

The second part includes what happens when the application is running. This part of the program is written in a while loop, involving logging measurements from sensors and writing instructions to output devices while the experiment runs. Each experiment lasts for an average of 20 minutes making the middle part the largest part of the application. This is where the casing control valve (CCV) exercises its control. The values of pressures, flowrates, and CCV opening are monitored in real-time. CCV is controlled using a case structure object that works like an if-else statement in a conventional programming language. CCV control is primarily achieved by

opening or closing the control valve to keep the pressure difference between the casing and the tubing at a specified value.

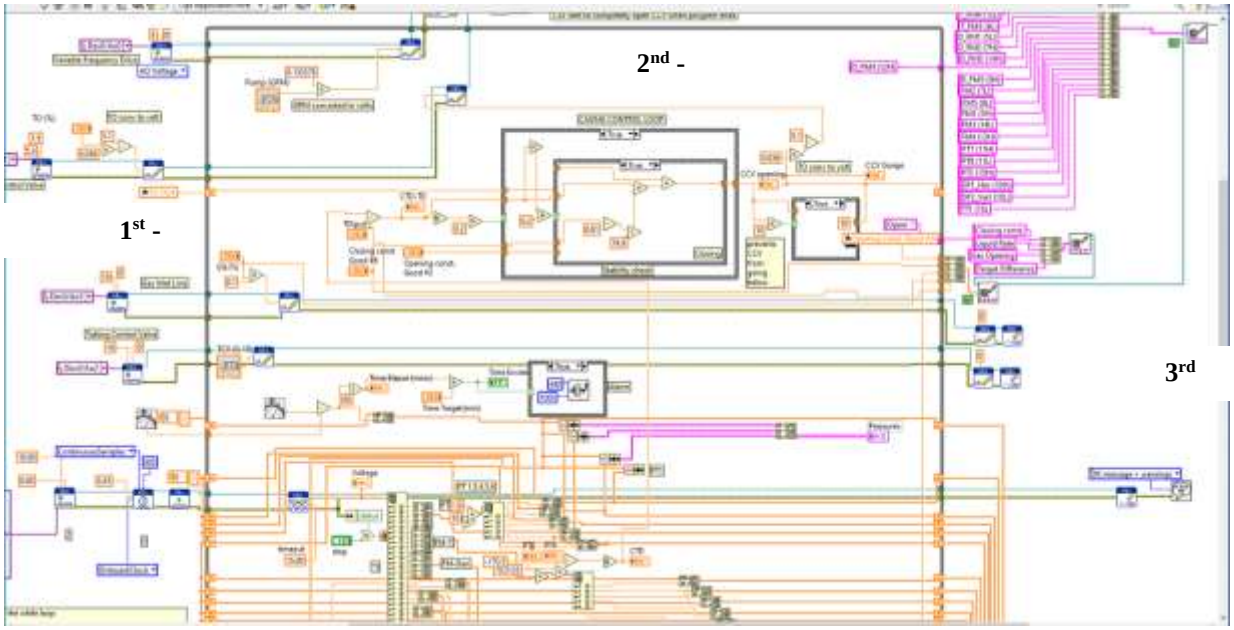

Figure 3.21. Block Diagram showing three sections

There are four controls on the CCV interface of the front panel shown in Figure 3. 19. The user must enter values for the closing constant, opening constant, target opening (TO) and target difference (TD). All four inputs are used in the CCV operation as explained by the equations used in closing and opening of the valve. The equations are written on an Integrated Development Environment (IDE) for simplicity of the if-statements. The first stage of the control line 4 of Figure 3.22 is to check whether the casing-tubing pressure difference varies from the target difference (TD), by a tolerance value of 0.2 psi.

```
3   CTD = PT-5 - PT-6
4  if TD - CTD > 0.2: #check if CTD is equal to TD
5      if TD > CTD + 0.2:
6          TO = TO + CTD - TD * (closing_constant - 0.01)/(75-0.1)
7  else
8      TO = TO + [CTD - TD] * opening_constant * 0.25
```

Figure 3.22. Casing Control Equations in LabVIEW

TO is the initial opening of the CCV, set to 30% based on the testing experience. Setting an initial opening close to the desired opening allows the slow-acting valve to stabilize the liquid level in the casing annulus rather quickly. The closing and opening constants in lines 6 and 8 control how fast the CCV opens or closes respectively. Good initial values are 2 for opening and 6 for closing. Increasing these values increases the rate at the which the valve closes or opens.

The last part of the developed LabVIEW application shown in Figure 3.21 deals with what happens when the experiment is stopped. It is activated by pressing the stop button on the front panel in Figure 3. 19. It includes the objects located outside the while loop at the top and right part of the application. It performs two main functions of shutting the voltage output from the computer to the equipment and writing the data logged from sensors to file. This section shuts down the pump and closes the gas inlet line, while it completely opens the casing control valve.

3.3. Test Procedure

In order to standardize and assure consistency in the conducted experiments, a general testing procedure was devised. This procedure was followed in a step-by-step manner for all of the conducted tests. The procedure for running the experiments is listed below in steps:

Step 1: Connect the computer, power box and DAQ card to the power sources. FM-1 and FM-2 have separate power cables that must also be connected to the power supply.

Step 2: Turn on the compressor and load after warm-up. Connect the air hose and secure the cam-locks using the attached pins.

Step 3: Power the VFD and press the reverse button followed by the run button.

Step 4: Close all the drain and bleed valves in the facility.

Step 5: Open the LabVIEW application front panel.

Step 6: Set the closing and opening constants, testing time target (minutes) – expected time to complete the test, TO, TD, GIL (%) and pump rate (GPM) on the front panel, shown in Figure 3. 19. Then, click the start button at the top right corner.

Step 7: Adjust closing and opening constants as needed until the liquid level in the casing annulus stabilizes, and the flow of liquids into the casing return line stops.

Step 8: It usually takes about 5 minutes for the liquid level to stabilize. Run the test for an additional 15 minutes to collect enough data points after the liquid level is stabilized.

Step 9: Monitor the casing return line for water flow during the test. Drain the casing return column when necessary. Stop the test if the CRL is about to be flooded or blown out due to excessive water influx.

Step 10: At the same time, watch the tubing return line for gas blowout. This occurs if the gas pushes the liquid level down in the casing. Immediately stop the test if this occurs.

Step 11: When the time target is elapsed, the "Time Exceeded" indicator on the front panel turns on and an alarm begins to beep signifying the end of the test.

Step 12: To stop the test, close the ball valve at the gas-liquid mixing tee. Then, press the stop button on the front panel to end the test.

Step 13: Power off the VFD

Step 14: Turn off the compressor and turn off the battery. Bleed air line at the GIL before removing the cam-locks from the compressor.

3.4. Text Matrix

Table 3. 3 and Table 3.4 show the test matrices for the centrifugal and gravity separators, respectively. A total of 7 gas rates and 24 liquid rates were tested for the centrifugal separator, covering a range of 17-855 bpd for liquid rate and 41-203 MSCF/D for gas rate. The test matrix was then shortened to 5 gas rates and 11 liquid rates for the gravity separator. The range of flowrates was forced by the facility limitations. Liquid rate of 17 bpd and lower were too low for the pump to run smoothly without turning off. Hence, only 41 MSCFD was tested at 17 bpd. In addition, it was difficult to control the CCV at gas rates higher than 203 MSCFD. A total of 155 tests were run for the centrifugal separator, with a total of 55 tests for the gravity separator. The analysis of the results will be presented in Chapter 4.

Table 3. 3. Centrifugal separator test matrix

Gas Flowrates (MSCF/D)	**Liquid Flowrates (BPD)**	
41	17.115	410.76
85	34.23	444.99
98	68.46	479.22
120	102.69	513.45
160	136.92	547.68
172	171.15	581.91
203	205.38	616.14
	239.61	650.37
	273.84	684.6
	308.07	753.06
	342.3	821.52
	376.53	855.75

Table 3.4. *Gravity separator test matrix*

Gas Flow Rate (MSCF/D)	Liquid Flow Rate (BPD)
41	68.5
98	136.9
120	205.4
172	273.8
203	342.3
	410.8
	479.2
	547.68
	616.1
	684.6
	753.1

CHAPTER 4: RESULTS AND ANALYSIS

This chapter provides a summary of the experimental results acquired in this study. First, the results are presented for a sample test to explain the experimental outputs and evaluation metrics. Then, the results are compared for various tests with the two tested separator types. The objective is to evaluate the performances of the separators at varying liquid and gas rates.

Each test is run for 20 minutes to record enough data under the stabilized flow conditions. Figure 4.1 shows the plots for a test conducted with liquid and gas rates of 171 bpd and 203 MscfD, respectively. Figure 4.1(a) shows the real-time pressure changes during the test at the entrance of the vertical section (PT-3), casing head (PT-5), and tubing head (PT-6). The reduction in pressure from PT-3 to PT-5 is due to the pressure losses in the vertical section as the mixture flows through the separator and is separated in the casing annulus. The difference between PT-5 and PT-6 is the main factor used to control the opening of the casing control valve, and hence, the liquid level in the casing.

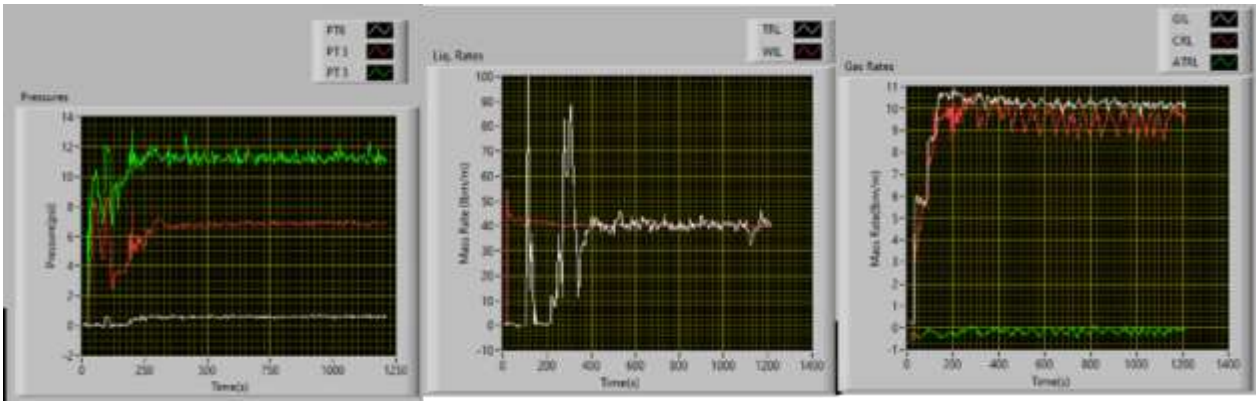

Figure 4.1. Real-time plots of (a) pressures; (b) inlet and outlet liquid flowrates; (c) inlet and outlet gas rates at 171 bpd of liquid and 203 MscfD of gas

Figure 4.1(b) is the real-time plot of the inlet (WIL) and outlet (TRL) liquid rates. The data is logged every 4 seconds. The TRL value is 0 until about 100 seconds when it rises rapidly, signifying the early period before the flow reaches the tubing return line. First flow in the tubing is followed by an early transient stabilizing at about 400 seconds. Figure 4.1 (b) reflects the three main parts of each test: (1) the period before the tubing starts to flow, (2) the transient period when the control valve tries to stabilize the liquid level in the casing and outlet liquid rate at the TRL, and (3) the period of stabilized flow in the tubing return line and constant liquid level in the casing annulus. Figure 4.1(c) shows the plots of gas flowrates at three locations: inlet (GIL), casing return line (CRL) and gas outlet at the tubing return line (ATRL).

The values from the ATRL meter, Figure 4.1(c), are mostly negative because of the low accuracy of the flowmeter for the gas flowrates encountered at the tubing return line. However, the flowrate at the meter can be inferred from the other two gas flowmeters. The measurement error chart of the 2" flowmeter is in the appendix, Figure A. 2. Most of the gas is produced from casing and usually less than 1 lb/min of gas is produced from the tubing even for the highest GLR test. The measurement error associated with this range of low flowrates at the ATRL in this study is about 25%. This explains the negative values measured in Figure 4.1(c) at flowrates close to 0

4.1 Separation Evaluation Metrics

4.1.1 Separation efficiency

The separators are evaluated based on gas and liquid separation efficiencies, and the variability of flowrates at the outlets. Two criteria are defined for calculating the gas separation efficiency: The first is shown in Eqn 4.1, defined as the ratio of the gas rate through the CRL to

the total gas inlet. The second is shown in *Eqn 4.2*, which is the ratio of the gas rate through the CRL to the total gas rates through the tubing and casing return lines (Lea and Garrett 2014).

$$Gas\ Eff.1\ = \frac{Casing\ Gas\ out\ (CRL)}{Total\ Gas\ in\ (GIL)} \qquad \textit{Eqn 4.1}$$

$$Gas\ Eff.2\ = \frac{Casing\ Gas\ out\ (CRL)}{Casing\ Gas\ out\ (CRL) + Tubing\ Gas\ out\ (ATRL)} \qquad \textit{Eqn 4.2}$$

$$Liq.Eff.= \frac{Total\ Liquid\ out\ (TRL)}{Total\ Liquid\ in\ (WIL)} \qquad \textit{Eqn 4.3}$$

Eqn 4.2 quantifies the proportion of the outlet gas rates that exits from the casing. It is a good indicator of separation efficiency, as an ideal downhole separator ensures that all of the gas is produced from the casing-tubing annulus and all of the liquid flows to the pump inlet.

Eqn 4.3 is the measure of liquid separation efficiency. It is the ratio of the total liquid produced from the tubing to the total liquid inlet. McCoy et al. (2015) identified three conditions that cause incomplete liquid fillage in pumps: gas interference, pumped-off conditions and pump intake obstruction. The efficiency of downhole separator should be evaluated only when gas interference is the cause of incomplete fillage, as the other two conditions cannot be fixed by downhole separators. The study performed by McCoy et al. (2015) on packer-type separators evaluates separation efficiency by comparing the inlet liquid fraction in the casing-tubing annulus to the liquid fraction in the pump, a similar indicator of liquid separation efficiency to the one defined by *Eqn 4.3*.

4.1.2 Outlet flowrate variability

A useful criterion for evaluating a downhole separator is the stability of liquid delivery to the pump inlet. Large pressure and flowrate fluctuations cause inefficient use of reservoir energy,

and may damage a well's production due to slugging and premature installation of expensive artificial lift equipment (Torre et al., 1987). Coefficient of variation is defined as shown in *Eqn. 4.4*, using the standard deviation and mean values for a set of data. It is used to quantify the fluctuation of liquid and gas flowrates at the inlet and outlet of the facility.

$$Coeff.of\ Variation = \frac{Standard\ dev.}{mean} \qquad \textit{Eqn. 4.4}$$

4.2 Centrifugal Separator Results

4.2.1 Visual Observations

Video recordings of flow behavior were taken by two cameras placed at the shroud inlet and the spiral outlet of the separator. The former is to show the sizes of gas bubbles and how they are drawn into the shroud, while the latter is to visualize flow behavior as the mixture exits the spiral section and pours into the casing-tubing annulus. Figure 4.2 is a screenshot taken at the shroud inlet, showing how the gas bubbles are drawn into the shroud to be produced from the tubing. The snapshot is from a test conducted at 98 MSCFD gas rate and 330 bpd liquid rate.

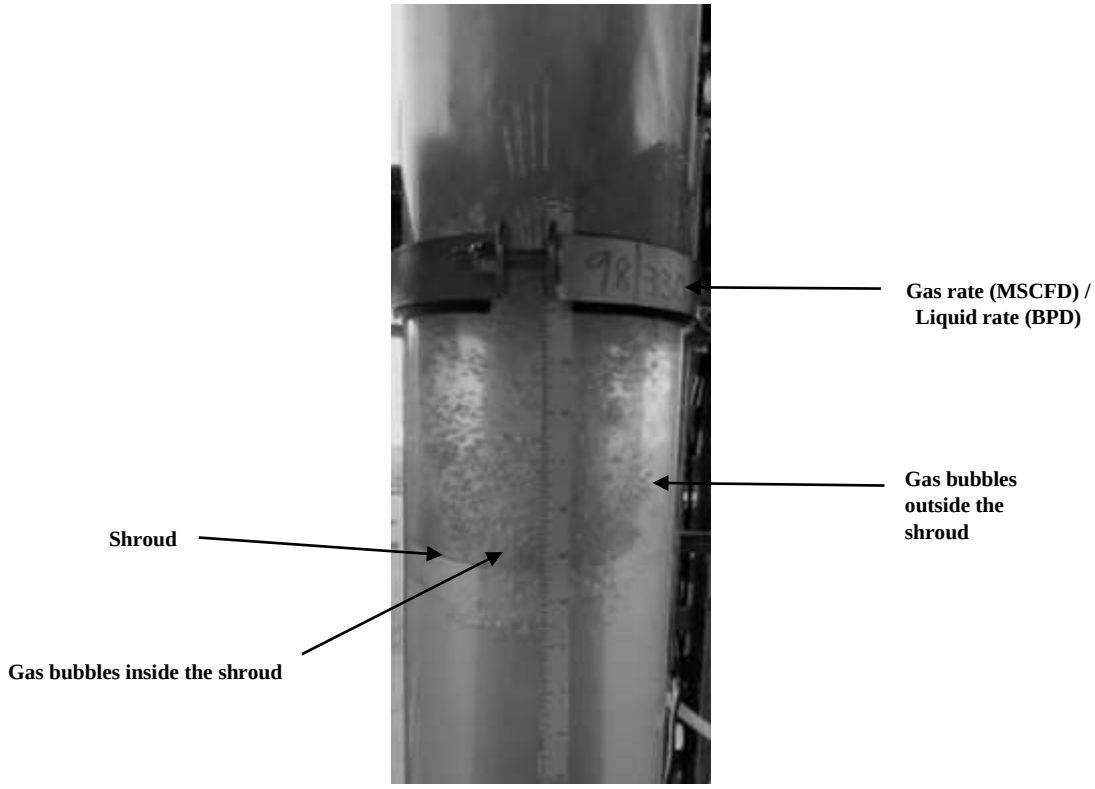

Figure 4.2 Shroud inlet visual observation

Gas bubbles are produced from the agitation of the mixture due to the change in flow direction from the separator into the annulus. After flowing out of the separator's spiral section, most of the gas bubbles flow upwards and break out of the liquid phase without getting down to the shroud inlet. However, low liquid level in the annulus and high liquid velocity could draw some gas bubbles down into the shroud inlet. These gas bubbles are generally small in size, as seen in Figure 4.2, and are the cause for the gas separation inefficiency.

Figure 4.3 is the visual observation at the spiral outlet as the liquid mixture leaves the separator. The spiral section of the separator imparts a centrifugal force on the mixture, affecting the flow profile as the mixture flows into the casing-tubing annulus. The liquid phase is affected more by the centrifugal force and is thrown to the walls of the casing.

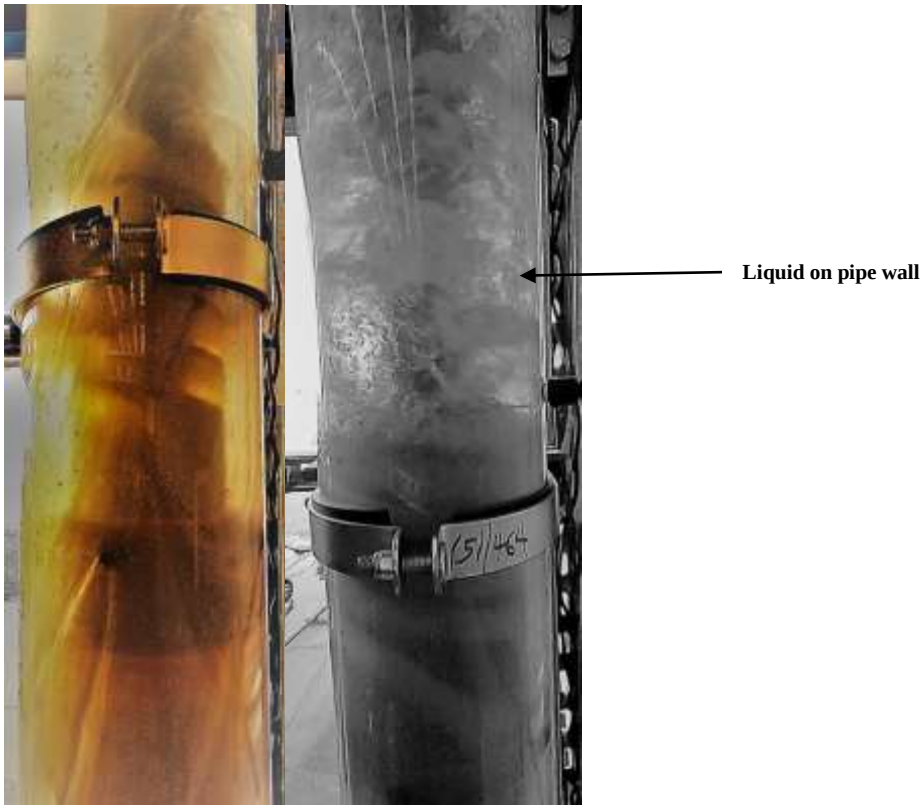

Figure 4.3 Spiral outlet visual observation

The effect of the centrifugal force results in liquid being thrown to the wall of the casing while gas remains at the center due to the density difference. This effect helps in the separation of the two phases as the gas occupying the central core flows upwards. The fraction of trapped liquid droplets in gas reduces, as the liquid loses velocity at the pipe wall and falls towards the shroud inlet for production at the tubing.

Figure 4.4 shows the liquid falling by the wall of the casing and displacing the gas bubbles in the annulus. The effect of this displacement on the separation of gas from liquid is unknown, and a function of liquid and gas rates.

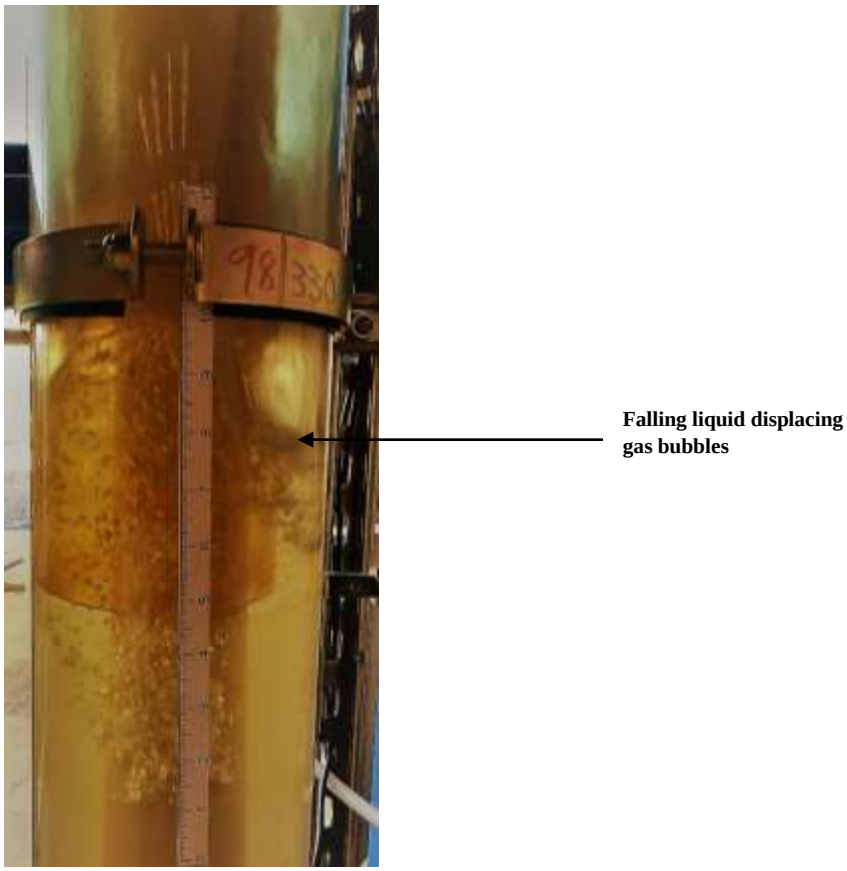

Figure 4.4 Falling liquid displacing gas bubbles above the shroud

The general liquid velocity profile in pipes shows that velocity is maximized at the middle of the pipe. In a downward falling liquid-gas mixture, where gas is constantly rising against gravity due to density difference, liquid falling by the pipe wall and displacing gas to the central core may reduce the slippage and result in increasing the downward velocity of the gas bubbles. Additional investigation is needed to verify the effect of this motion on bubble velocity around the shroud.

4.2.2 Experimental Measurements for Centrifugal Separator

Three sets of plots were generated for each test to better understand the effects of liquid and gas flowrates on separation efficiency. These plots include the following:

1. Mass rates of liquid at the inlet line (WIL) and the tubing return line (TRL) plotted against time in seconds. These plots are shown in the first row of Figure 4.5 for an example test

with 203 Mscf/D of gas and 171 bpd of liquid.

2. Mass rates of gas at the inlet line (GIL), casing return line (CRL), and the summation of casing and tubing return lines (CRL + ATRL) plotted against time. These plots are shown in the second row of Figure 4.5 for the same example test. The summation of ATRL and CRL gives the total gas outlet from the test section, and should ideally be equal to GIL.
3. Pressures at the casing head (PT5) and tubing head (PT6) plotted against time. These plots are shown in the third row of Figure 4.5.

The three columns in Figure 4.5 represent three time periods considered in the plots and analysis. These time periods are as follows:

1. The first column shows the data spanning the whole duration of the experiment. This is approximately 20 minutes or 1200 seconds for most tests.
2. The second column shows the data starting at the onset of flow at the tubing return line. This is the time at the start of liquid production at the tubing return line.
3. The third column begins when the flow is stabilized in the casing annulus. This is the steady state period, starting from the point that liquid level is controlled in the casing annulus. The steady state was established using the following criteria:
    a. The hydrostatic head in the tubing above the separator (implied by the difference between casing head pressure and tubing head pressure, PT5 – PT6) is greater than 5.6 psi, equivalent to approximately 13 ft of water. And,
    b. The difference between inlet and outlet liquid rates is less than 2 lbm/min (8.2 bpd).

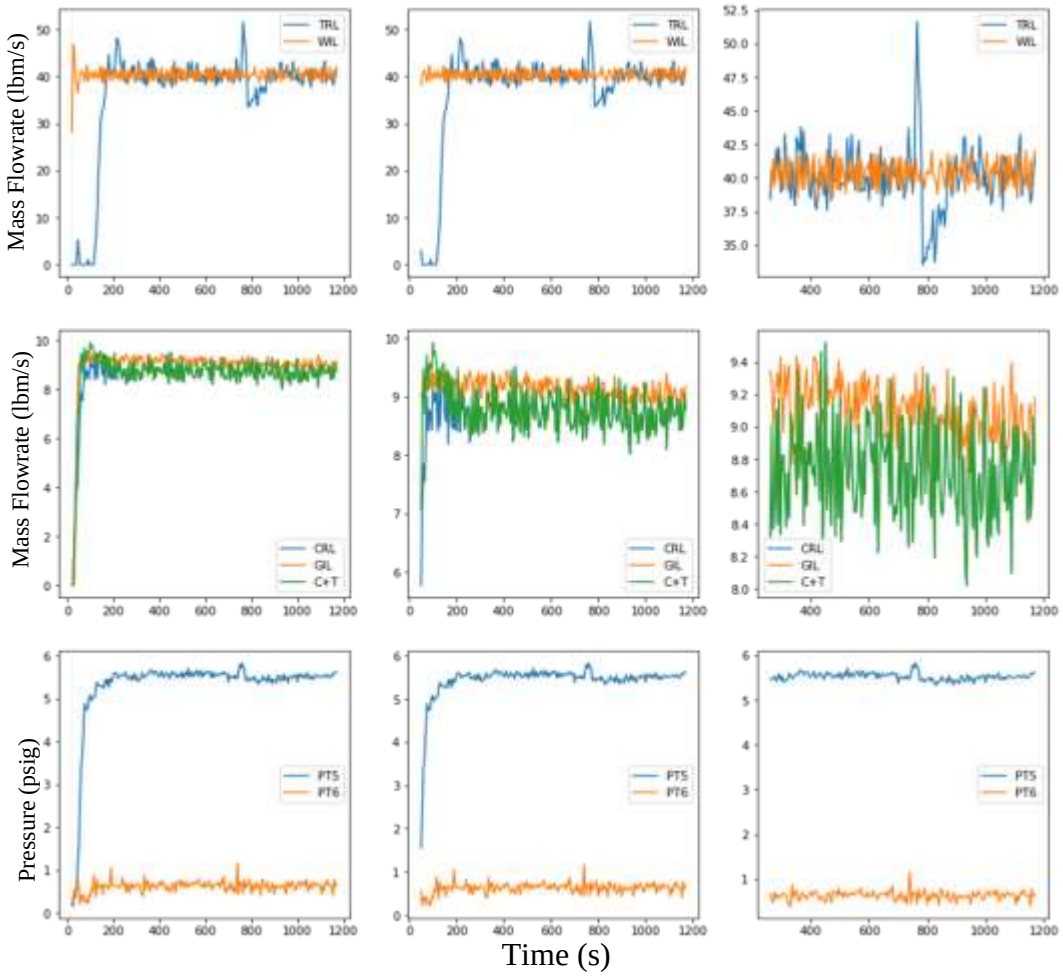

Figure 4.5 Experimental results for a test with 203 Mscf/D of gas and 171 bpd of liquid

Liquid separation efficiency values were considered as the primary means of evaluating the separator's performance because of the lower associated errors for the measurements of the liquid flowmeters compared to the gas flowmeters. For example, in case of the test shown in Figure 4.5, measurement errors in ATRL flowmeter sometimes result in gas separation efficiencies higher than 1, when using Eqn 4.2. Figure 4.5 shows the need for considering steady state conditions in evaluating the separator's efficiency. The results show lower liquid separation efficiencies for the unsteady and first-flow periods compared to the steady state case. This is because of the initially unstable liquid levels resulting in liquid being carried over to the casing head. Once the liquid level in the casing is controlled, the only way for liquid carryover is in form of small droplets dispersed

in the gas core.

4.2.3 Separation Efficiency Analysis

The liquid separation efficiency was higher than 90% in steady state conditions for most of the conducted tests. The optimum range with the highest separation efficiency was within 5 to 20 gpm (171-685 bpd) for all the gas rates tested. The efficiency dropped at liquid rates below 5 gpm (171 bpd) especially at high gas rates (greater than 58 Mscf/D, Figure 4.6). This is due to high gas velocities increasing the upward drag on liquid droplets towards the casing head.

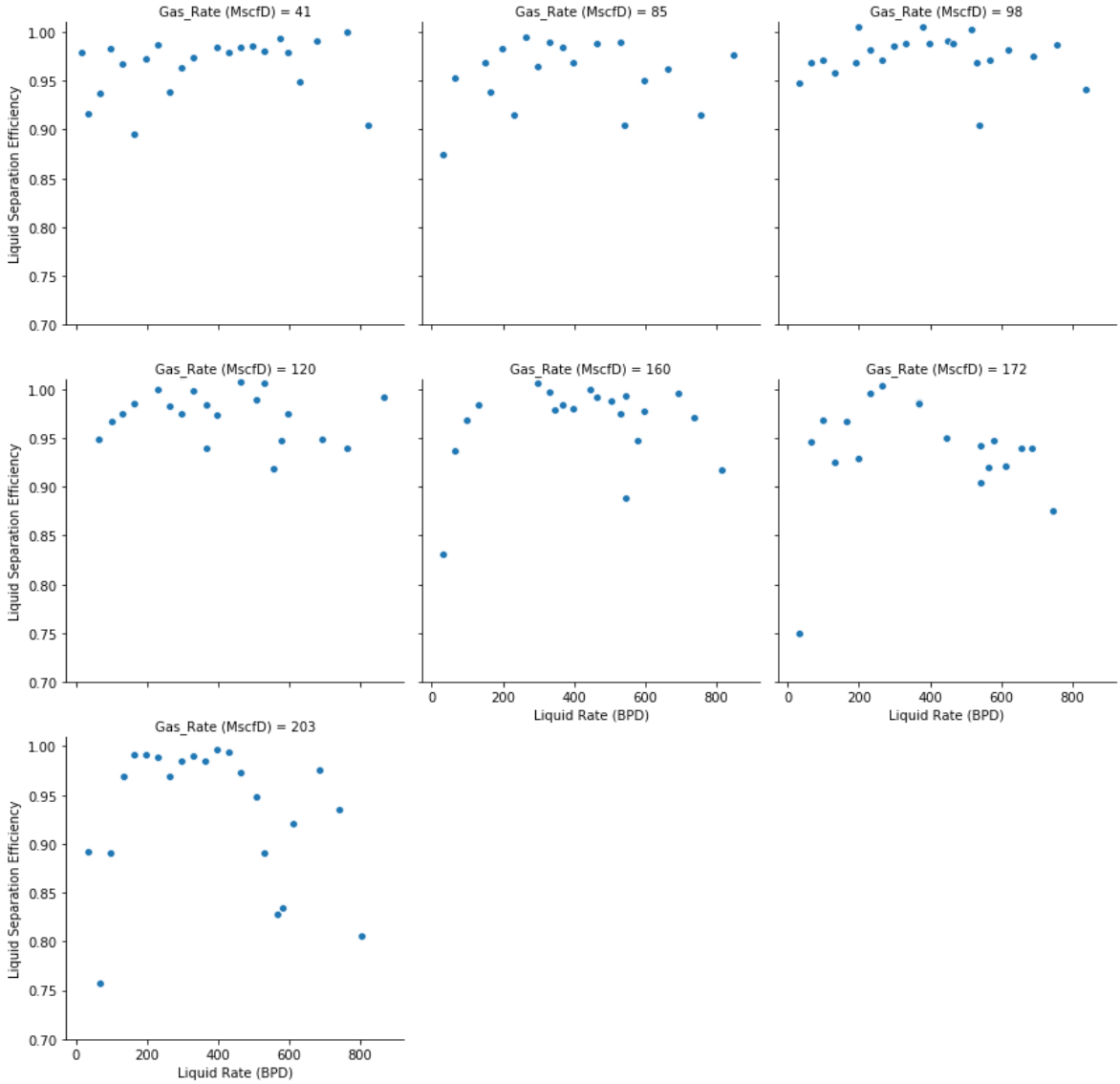

Figure 4.6. Liquid separation efficiency with liquid flowrate at the 7 tested gas rates

Figure 4.6 reveals that separation efficiency is both a function of the liquid rate and the gas rate in the mixture. At liquid flowrates higher than 20 gpm (685 bpd), liquid separation efficiency dropped because of the increase in annular liquid velocity. Under these conditions, the kinetic energy of the mixture exiting the spiral section does not dissipate enough to allow all the liquid to fall into the shroud inlet and be produced via the tubing. Liquid chunks flow up the casing dragged by the gas flow. The higher the gas rate, the more liquid it carries to the casing head. Gas separation efficiency also drops because of liquid dragging larger bubbles into the shroud. Studies by (J. M. McCoy et al., 2007) state that good gas separation is not guaranteed even at annular liquid velocities below 6 in/s, if the annular gas velocity exceeds 7-8 in/s.

4.2.4 Outlet Liquid Variability

Eqn. *4.4* is the coefficient of variation that quantifies fluctuation in a dataset, such as flowrate, with time. During the experimental campaign, it was used to make decisions on repeating a test or eliminating duplicates in repeated tests. The test with the lowest coefficient of variability at the liquid outlet was selected as the final test for a given pair of liquid and gas rates.

Figure 4.8 shows the distribution of the fluctuation of liquid production at the outlet and compares it with the fluctuation of inlet liquid flowrate at the pump. The maximum fluctuation at the inlet (excluding the outliers) is less that the 25th percentile of the outlet flowrate, which is 25 bpd. This shows that the pump does not contribute to the fluctuation of liquid flowrate at the outlet.

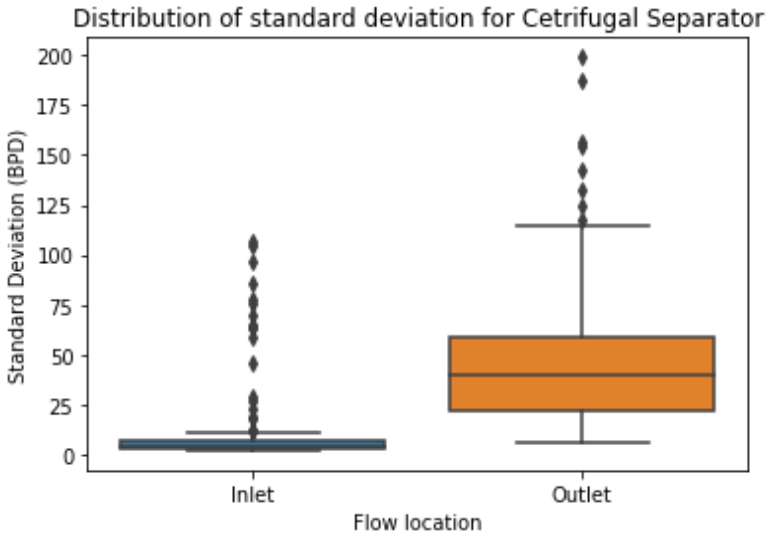

Figure 4.7. Distribution of standard deviation for centrifugal separator

Figure 4.8 is the plot of coefficient of variation at the liquid outlet for all the tests performed on the centrifugal separator at varying liquid and gas flowrates. The trend shows that the variation of produced liquid decreases as the gas rate increases. This observation is more pronounced by observing the trend in each plot at liquid rates less than 400 bpd.

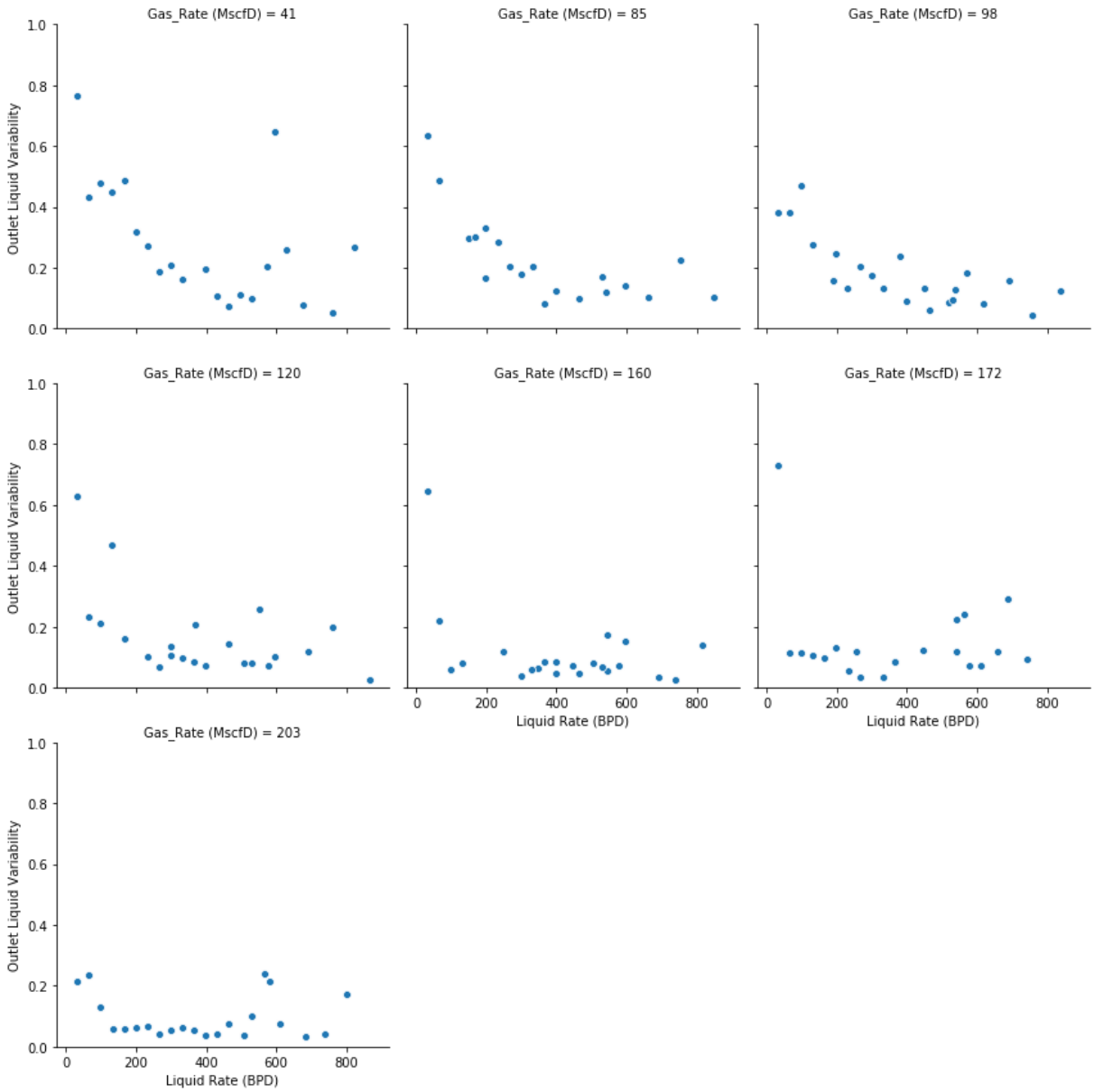

Figure 4.8. Variability plot for all tests (Centrifugal separator)

Decrease in the slope of the trend of variation from 41 MscfD to 203 MscfD in Figure 4.8 shows decreasing fluctuation of produced liquid as inlet gas rate increases. Figure 4.9 shows the distribution of the coefficient of outlet liquid variation for all the gas rates tested. The distribution and median of the fluctuations decrease as the gas rate increases. This observation is consistent with the general knowledge that intermittent flow in risers occur at low gas and liquid rates.

Increasing the gas rates increase the energy of the system and shortens the cyclic period of the stream, hence reducing the fluctuations.

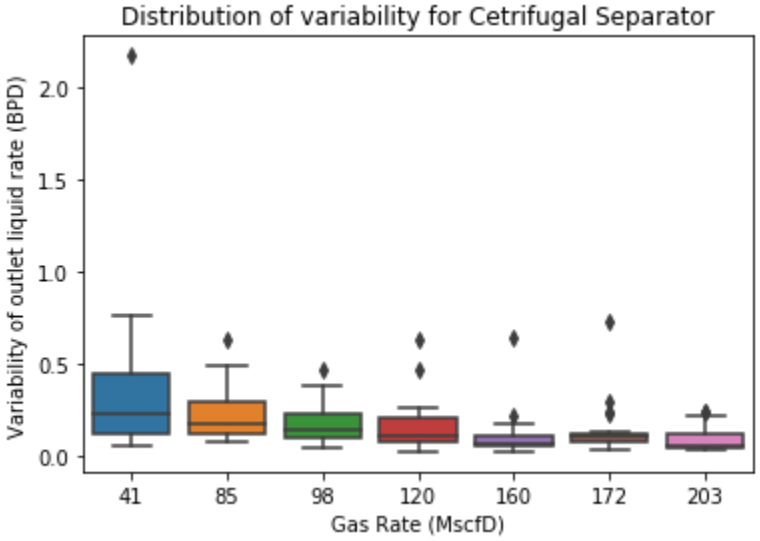

*Figure 4.*9. Distribution of *liquid variability* for all gas rates

4.2.5 Efficiency and Variability

Figure 4. 10 shows an error plot of efficiency and coefficient of variation at varying gas and liquid flowrates. The error bar for each data point is the coefficient of variation of the outlet liquid flowrate for the flow condition represented. The left y-axis is the liquid separation efficiency in percentage while the right y-axis is the coefficient of variation multiplied by 20 for outlet liquid. A factor of 20 was used to magnify the order of coefficient of variation to that of the separation efficiency for easier visualization. Coefficient of variation was selected over standard deviation in order to normalize the natural effect of increasing standard deviation as the size of data increases.

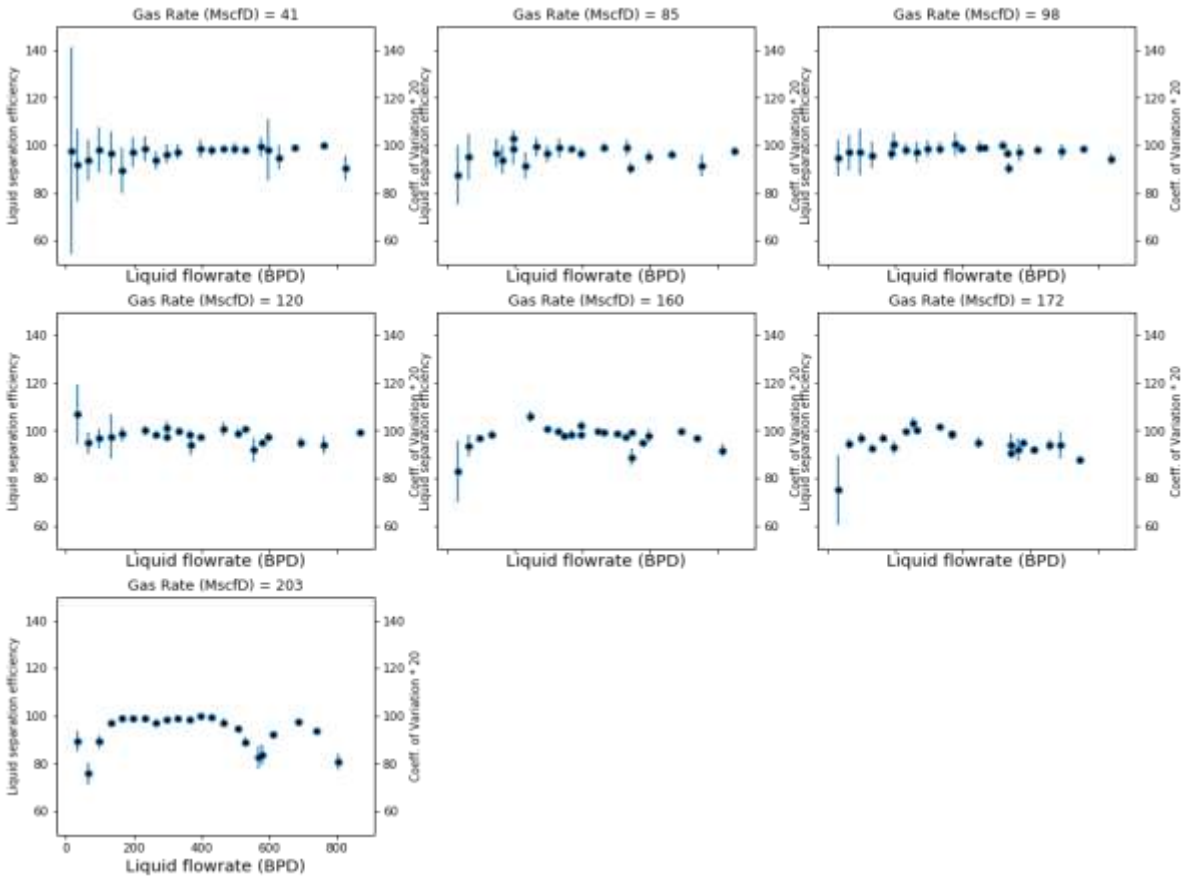

Figure 4. 10. Efficiency and coefficient of variation of outlet liquid flowrate

Two major trends are observable in Figure 4. 10. Variation decreases as liquid rates increases for the same gas rate. Similarly, variation reduces as the gas rate increases for the same liquid rate. This is consistent with literature that production fluctuation occurs at low superficial gas and liquid velocities (Torre et al., 1987).

4.2.6 Liquid Level Effects

The difference between casing and tubing pressures was used to control the casing liquid level around the level of the separator. After conducting the first test matrix, shown in Table 3. 3, a shortened set of experiments was conducted to analyze the effects of liquid level in the casing annulus on the separator's performance. For this purpose, the target difference between casing and tubing pressures (PT5 – PT6) was reduced to 5.5 psi from the initial 6.3 psi. Decreasing the target

pressure difference increases the opening of the casing control valve to reduce the backpressure on the casing annulus. This consequently increases the liquid level in the annulus. Considering the casing-tubing system as a U-tube, a change of target pressure difference from 6.3 to 5.5 psi would result in a 22-inch increase in casing liquid level. An overall of 36 experiments were conducted with a target pressure difference of 5.5 psi. The results are presented in Figure 4. 11 as red markers, compared to the earlier tests shown by blue markers.

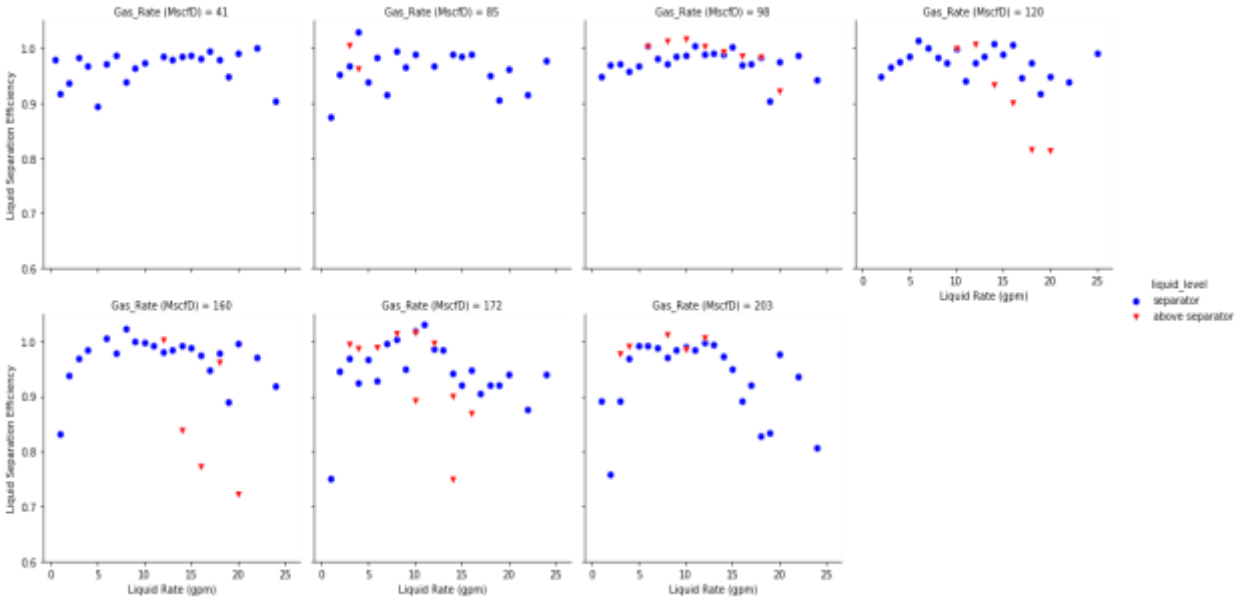

Figure 4. 11. Effects of liquid level in the casing annulus on liquid separation efficiency

Due to the difficulties to control the liquid level at approximately 2 feet above the separator outlet level and a smaller number of completed tests, it is hard to draw any solid conclusions from Figure 4. 11. However, it can be observed that liquid separation efficiency drops even further with higher liquid levels at high gas rates. The turbulence at high gas rates causes more liquid carryover to the casing head, reducing the separator's efficiency. The casing unit used in this study's experimental setup is only 27 ft long and the separator spiral outlet is located 16 ft from the casing head. With the liquid level closer to the casing head, it is easier for high velocity gas to carry the liquid over into the casing return line, reducing the liquid separation efficiency. High liquid level

in the casing annulus theoretically improves a pump's performance in the tubing since the head will ensure adequate pump fillage. This needs to be further verified by analyzing the gas separation efficiency of the separator.

4.2.7 Observations from Low Gas Rate Experiments

Figure 4. 12 shows the effect of liquid flowrate on a typical test with a fixed gas flowrate of 41 Mscf/D. The plots show the flow rates of liquid at the inlet (WIL) and the tubing return line (TRL) with time. A constant liquid rate at the tubing return line implies smooth production with no fluctuations. From the plots, slugging frequency and severity at the return line decreases with increasing the liquid rate up to 480 bpd. Beyond this liquid rate, slugging severity increases again because of the casing liquid level instability.

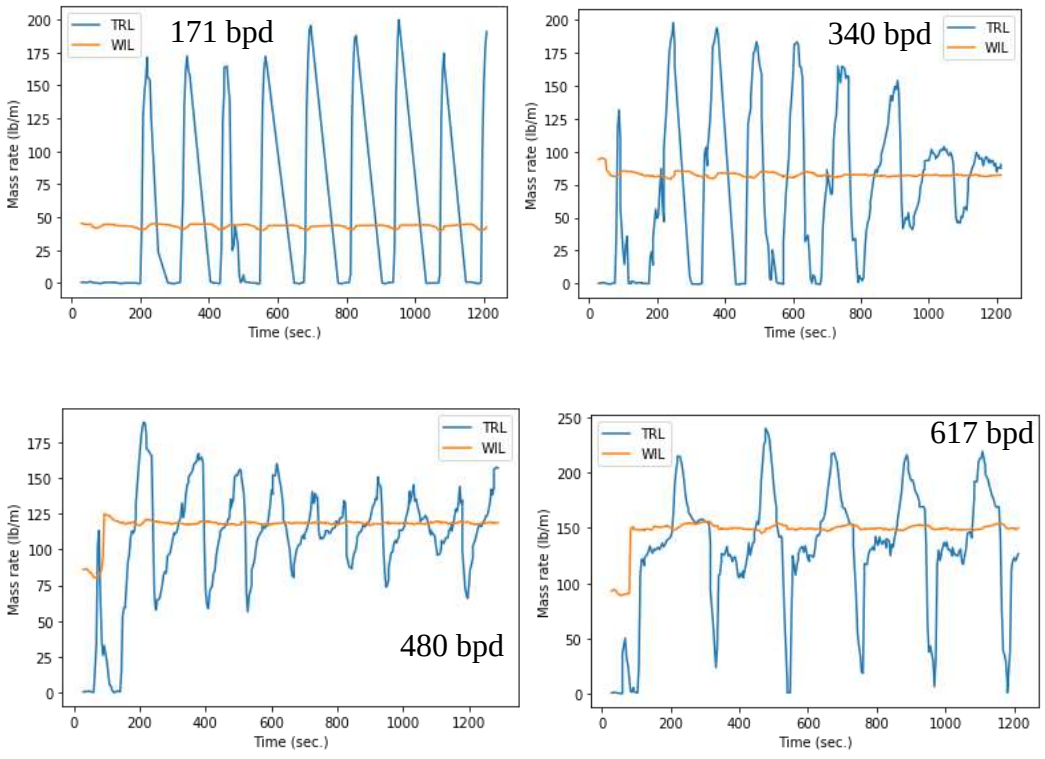

Figure 4. 12. Liquid inlet and outlet rates with time at a gas rate of 41 Mscf/D

4.2.8 Pressure Drop Across the Centrifugal Separator

Figure 4.13 shows the pressure drop across the separator at different gas and liquid flowrates. Expectedly, pressure drop across the separator increases with increasing gas and liquid flowrates. This is because of the increase in the velocity and frictional pressure drop as the fluids pass through the separator and the spiral section when the gas rate increases. The findings of (McCoy et al., 2005, 2007, 2015) indicate that pressure drop across a downhole separator should be minimized to prevent gas breakout in the separator, which reduces liquid fillage in the pump. PVT calculations need to be conducted to quantify the amount of gas evolved from the liquid because of a given pressure drop across the separator.

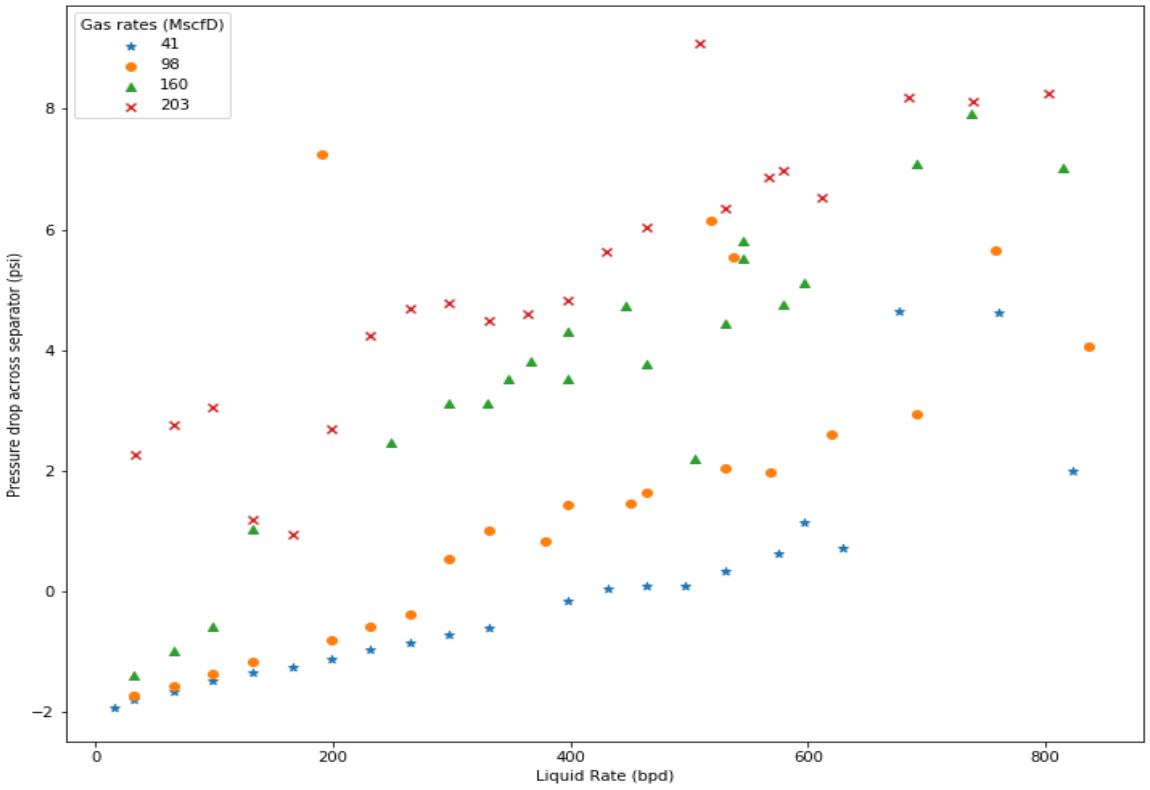

Figure 4.13. Liquid Flowrate versus Pressure drop across separator (PT3-PT4)

Some negative pressure drop values are observed for low liquid and gas rates in *Figure 4.13*. *Figure 4.14* is the schematic of fluid movement in a downhole separator. The force balance of the schematic is given by Eqns. 4.5 to 4.7 to explain the condition where PT4 can be higher than PT3.

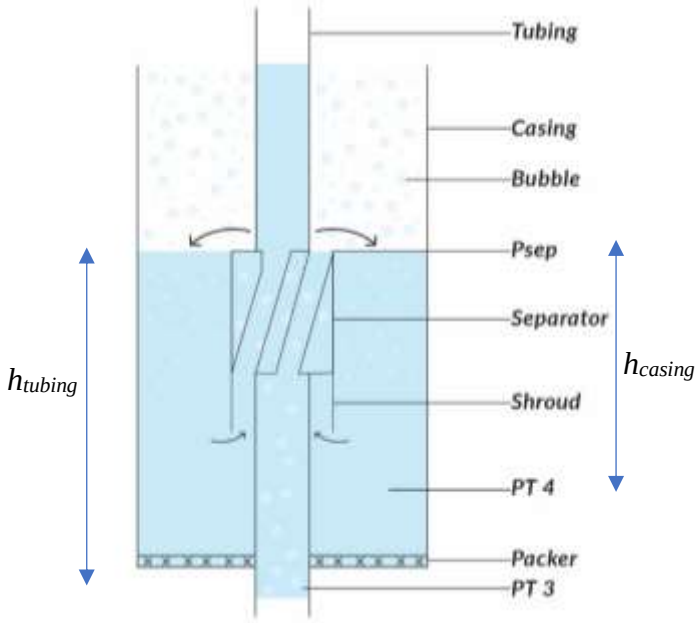

Figure 4.14. Packer-type separator schematic

$$PT4 = P_{sep} + \rho_{casing} g h_{casing} \qquad \textit{Eqn. 4.5}$$

$$PT3 = P_{sep} + \rho_{tubing} g h_{tubing} \qquad \textit{Eqn. 4.6.}$$

$$PT3 - PT4 = \rho_{tubing} g h_{tubing} - \rho_{casing} g h_{casing} \qquad \textit{Eqn. 4.7}$$

The above equations are developed by neglecting the frictional pressure losses across the separator. Eqn. 4.7 becomes negative when the hydrostatic head in the casing is higher than the tubing. This occurs at low liquid rates when the inlet tubing liquid holdup values are low, making the fluid column in the tubing lighter than the casing. The casing annulus is filled mostly with liquid below the spiral level, as it is placed after the separator. On the other hand, two phases always exist in the tubing leaving room for eqn. 4.7 to be negative at low liquid flowrates.

Figure 4.15 shows the bubble plot of pressure drop across the separator, the size of the bubbles is proportional to the magnitude of the pressure drop. The areas of the plot with no data plotted indicate insignificant pressure drop values. The plot shows an increase in pressure drop to the left and top of the plot signifying an increase in pressure drop as gas and liquid rates increase.

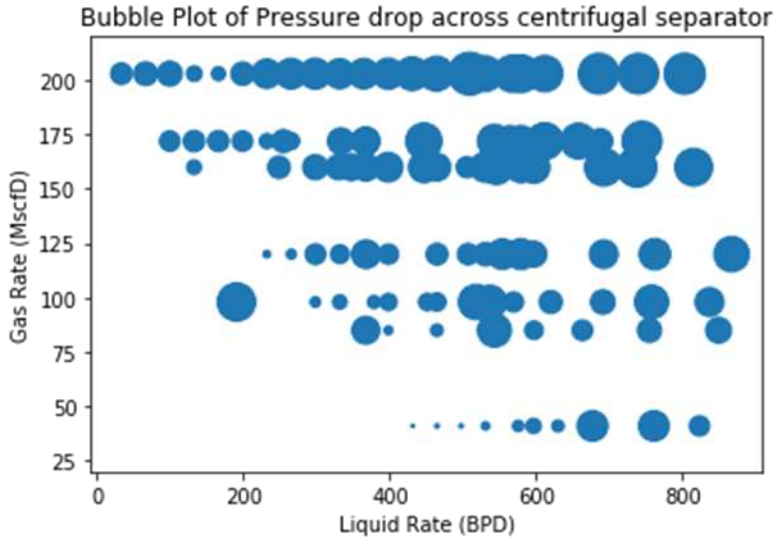

Figure 4.15. Bubble plot of pressure drop across separator

Figure 4.16 is a plot of liquid separation efficiency against pressure drop across the separator. While the observed trend is not strong, the plot suggests that liquid separation efficiency decreases with increasing pressure drop across the separator. Pressure drop across the separator is an important factor affecting the separation efficiency. As seen from the plots, increases in gas and liquid rates increase the pressure drop across the separator and in turn lower the separation efficiency. The lowest separation efficiency recorded for the Echometer packer-type separator is at a gas rate of 203 Mscf/d.

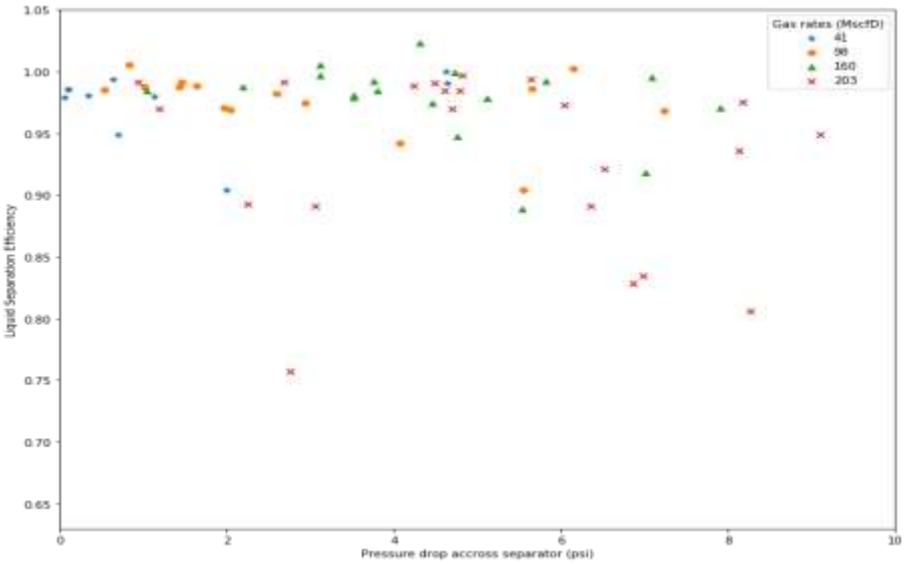

Figure 4.16. Liquid separation efficiency vs. pressure drop across the separator (PT3 – PT4)

4.3 Basic Gravity Separator Results

The gravity separator, shown in Figure 3.11, is a replica of the centrifugal separator except for the absence of the spiral part and the reduced length. A total of 55 tests were run on the gravity separator. The test matrix is given in Table 3.4 and the results are presented in the next sections.

4.3.1 Visual Observations

Figure 4.17was taken at the outlet of the gravity separator as the mixture enters the casing annulus. Unlike the centrifugal separator, shown in Figure 4.3, the liquid phase is not thrown to the wall since the gravity-type separator does not have the spiral section to provide the centrifugal effect. Liquid and gas phases are separated merely by gravity, as they pour into the casing.

Figure 4.17. Visual observation of the gravity separator outlet

Figure 4.17 shows that the fluid exiting the separator is a homogeneous mixture of gas and liquid, ultimately separated in the annulus. The effect of the gravity-type separator is that it increases the velocity of the mixture as it flows through it and creates agitation, which is favorable for separation of two phases with density difference when the velocity drops in the casing annulus due to a larger area of flow than the separator area. In the casing-shroud annulus, the liquid phase loses energy and falls to the shroud inlet while the lighter gas flows upward towards the casing head. The back pressure provided by the casing head facilitates liquid fall back in the annulus and enhances separation.

Figure 4.18 shows the shroud inlet for both centrifugal-type and gravity-type separators with the same gas rate of 203 MSCFD but slightly different liquid rates of 170 bpd and 205 bpd, respectively. In both cases, bubbles are being dragged by the liquid phase into the shroud, but the bubble sizes differ for the two separators.

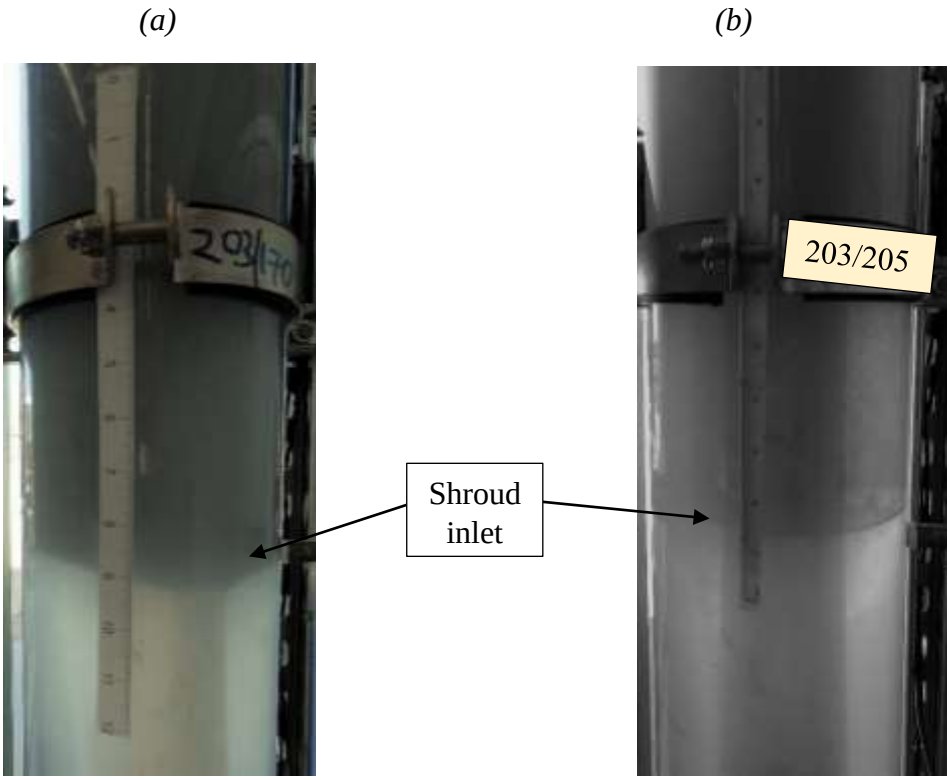

Figure 4.18. Gas bubbles at shroud inlet (a) Centrifugal separator (b) Gravity separator

The bubbles generated by the centrifugal separator in Figure 4.18(a) are smaller than those of the gravity-type separator in Figure 4.18(b). This means larger bubbles are separated before getting to the shroud inlet of the centrifugal separator, improving the separation efficiency. Also, there are more bubbles around the shroud for the centrifugal separator, and therefore, the shroud inlet is clouded and not as visible as it is for the gravity separator. Both of these tests resulted in high separation efficiencies, with a value of 98.7% for the centrifugal separator and 99.7% for the gravity separator.

4.3.2 Gravity Separator's Efficiency Results

Figure 4.19 shows the liquid separation efficiency of the basic gravity separator at different liquid and gas rates. The three lowest gas rates are dominated by very high separation efficiency values, while the separation efficiency decreases at high liquid rates for 172 and 203 MscfD of gas rates.

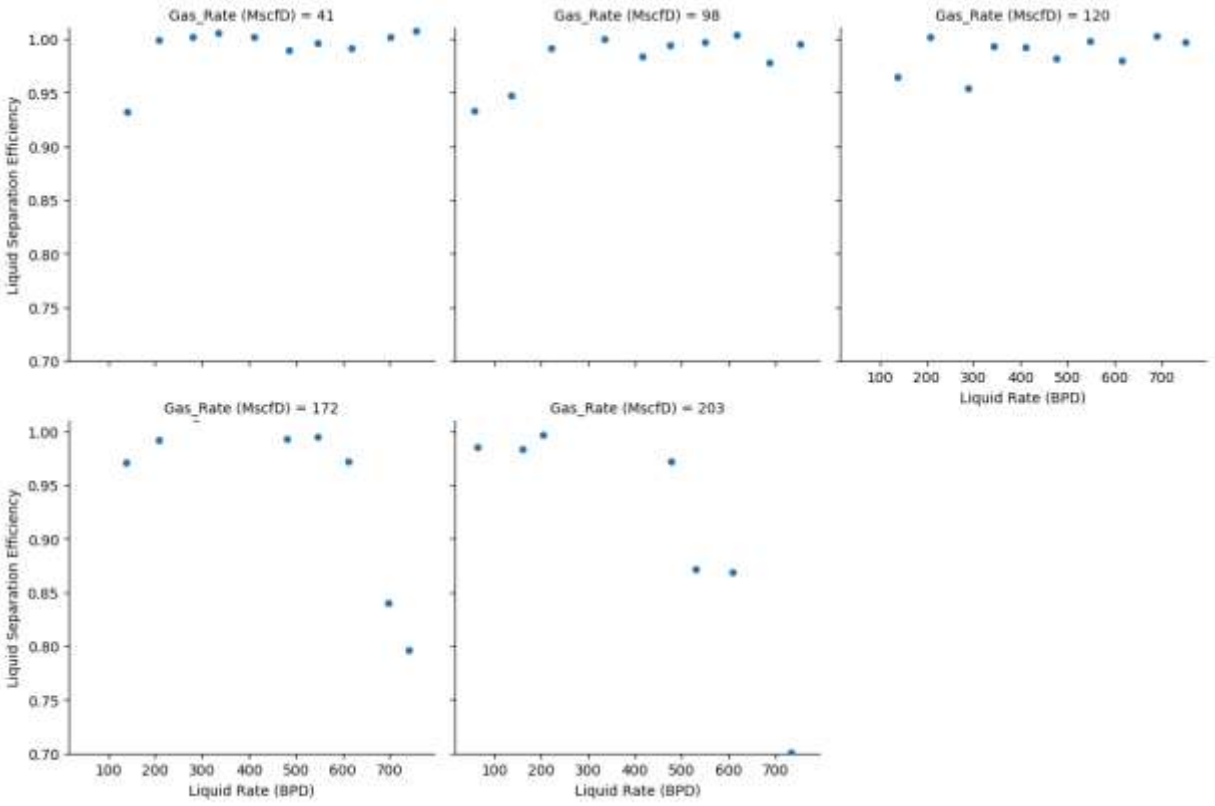

Figure 4.19. Liquid separation efficiency for Gravity separator

Figure 4.20 is the plot of the mean liquid separation efficiency for the gas rates presented in Figure 4.19. The trend shows that the average liquid separation efficiency reduces as the gas rate increases. Hence, the highest gas rate, 203 MscfD, has the lowest mean liquid separation efficiency at approximately 88%.

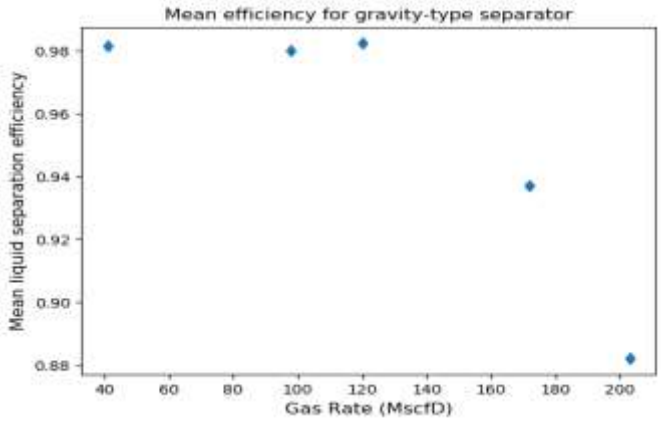

Figure 4.20. Mean liquid separation efficiency with gas rate for gravity-type separator

4.3.3 Liquid Output Variability of Gravity-Type Separator

Figure 4.21 shows the distribution of flowrate fluctuations at the inlet pump and at the tubing return line. The plot shows very high fluctuation at the tubing return line compared to the pump. The inlet pump used for the tests is a Moyno pump, which can show some fluctuations, particularly at low flowrates. However, these fluctuations are negligible relative to the variation observed at the tubing return line.

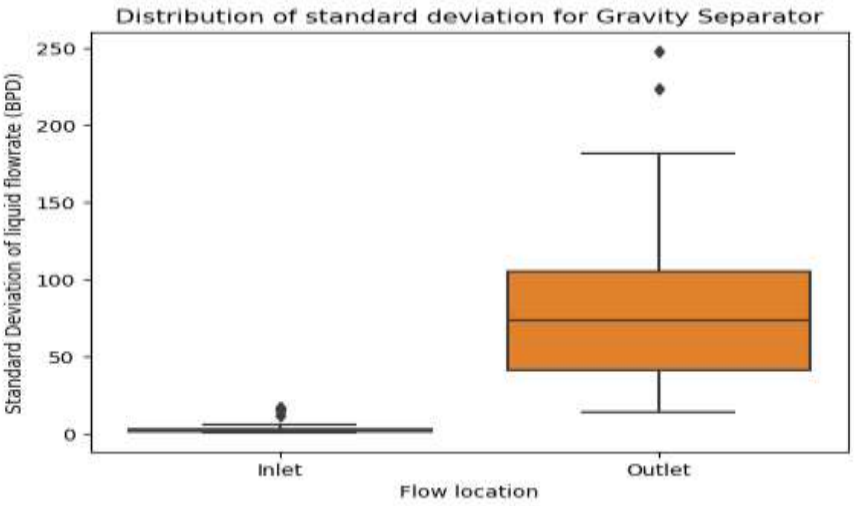

Figure 4.21. Standard deviation distribution for gravity-type separator

The distribution shows that fluctuation of flowrates at the inlet pump is generally less than 10 bpd, showing the reliability of the pump in delivering constant flowrates throughout the tests. The distribution of the output liquid flowrate fluctuation with gas rate is shown in Figure 4.22. The y-axis is the standard deviation in bpd, while the x-axis shows the 5 gas rates examined. The flowrate fluctuation decreases as the gas rates increase, implying a smoother separator output. The highest fluctuation of flowrate at the tubing return line is observed at 41 MscfD. Outlet liquid flowrate at this gas rate varied by as high as 250 bpd while running a test. This is because of the increased slugging at low gas rates, and the inability of the gas phase to keep a constant liquid level in the casing.

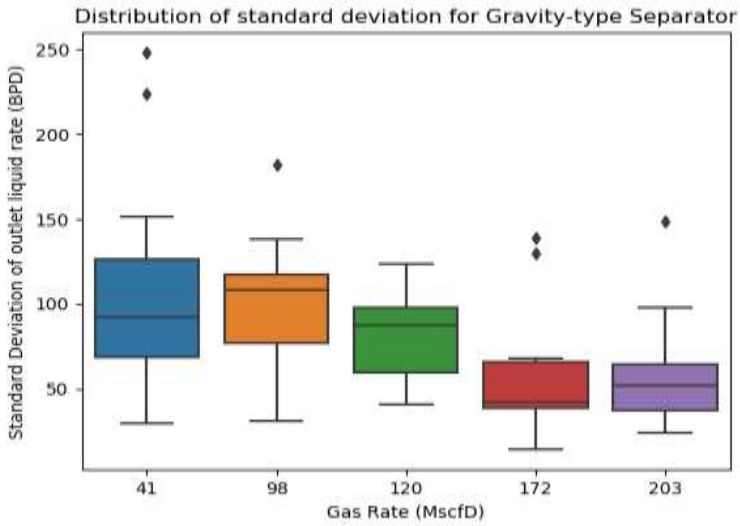

Figure 4.22. Standard deviation distribution for gravity-type separator

4.3.4 Gravity Separator Efficiency and Variability

A combination of separator's efficiency and fluctuation of liquid production output is shown in Figure 4.23. The form of the plot is similar to the error plot explained in section 4.2.5 with the error bars showing the magnitude of the variation coefficient for each test. The highest

fluctuations are observed at 41 MscfD which is the lowest gas rate while the lowest fluctuations are at high gas rates.

While liquid separation efficiency values are high for all the tests, measuring above 90% efficiency at 41 MscfD, it is important to consider the high fluctuation of liquid production as well. While some tests at 172 and 203 MscfD have relatively lower efficiency, liquid production at these conditions are more stable.

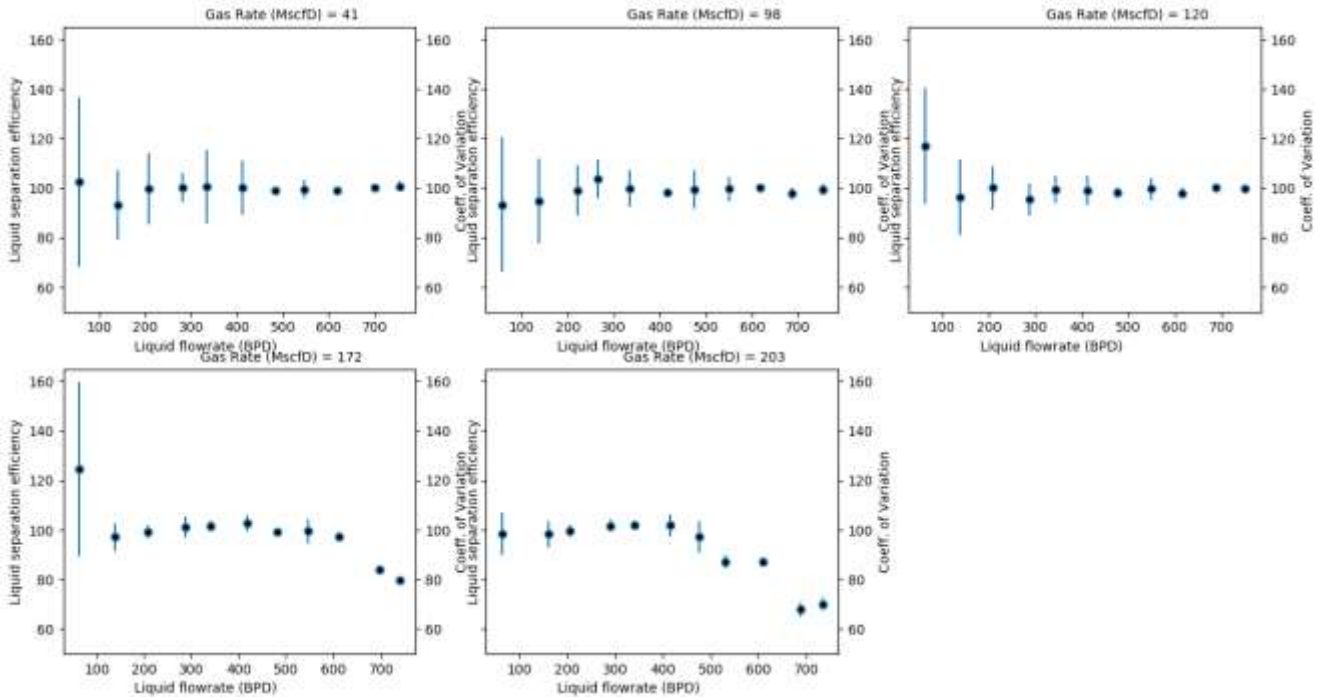

Figure 4.23. Efficiency and variability plot for gravity separator

4.3.5 Pressure Drop Across Gravity Separator

Pressure drop across the gravity-type separator is plotted in Figure 4.24 for all gas rates examined. The general trend of the plots is an increase in pressure drop as liquid flowrate increases for every gas rate, except for the tests at 203 MscfD with liquid rates greater than 600 bpd.

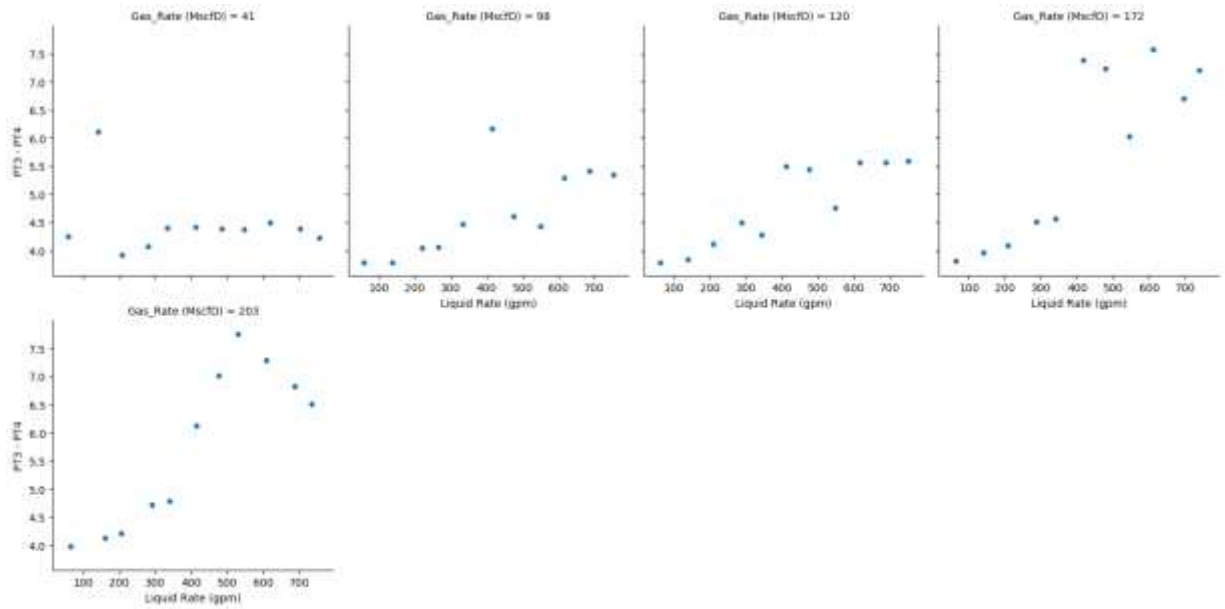

Figure 4.24. Pressure drop across gravity-type separator

At the gas rate of 203 MscfD, pressure drop linearly increases with liquid flowrate until 600 bpd before it begins to decline. The likely reason for this is the change in the target pressure difference used to control the casing control valve and stabilize liquid level in the casing annulus at these flowrates. Target difference of 6.3 psi was used at 530 bpd, but it was increased in 0.1 psi steps to 6.6 psi up to 734 bpd, which is the last data point. TD was increased to maintain liquid level at the spiral outlet at high flowrates. The increase in TD increases backpressure on the casing annulus, which in turn reduces the pressure loss across the separator. This is the likely reason for the unusual trend in the pressure drop at 203 MscfD.

4.4 Comparison between Centrifugal and Gravity Separators

The performances of the centrifugal-driven and gravity-driven separators are compared in this section. The gravity-driven separator was tested over 55 combinations of flowrates, while the centrifugal separator was tested over a range of 151 flowrates. To compare the results obtained

from both separators, the 55 test conditions that the two separators have in common was used. Figure 4.25 is a boxplot showing the distributions of both the coefficient of variation and standard deviation of produced liquid at the tubing return line for each separator. Neglecting the outliers, centrifugal separator provides a lower fluctuation in liquid output, with most of the deviations lower than 50 bpd.

This observation implies that the centrifugal separator has a more stable liquid production than the gravity-type separator. The centrifugal separator is less susceptible to intermittent production and the accompanying negative effects like reduced pump efficiency, flooding surface equipment and lost production in periods of no-flow.

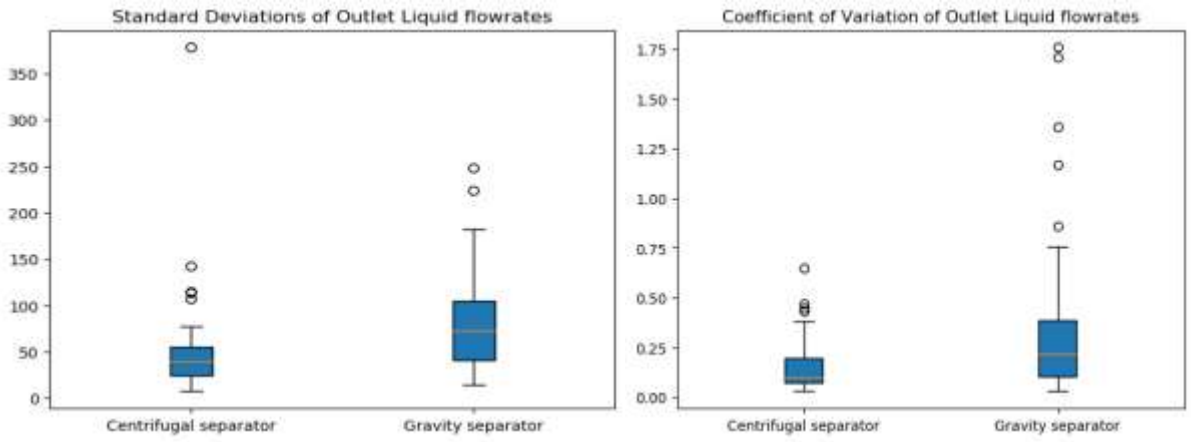

Figure 4.25. Comparison of standard deviation of outlet liquid flowrates

Figure 4.26 shows the comparison of liquid separation efficiency between the two separators. The results are comparable for the two separators and the difference between them are within the uncertainty ranges of the tests.

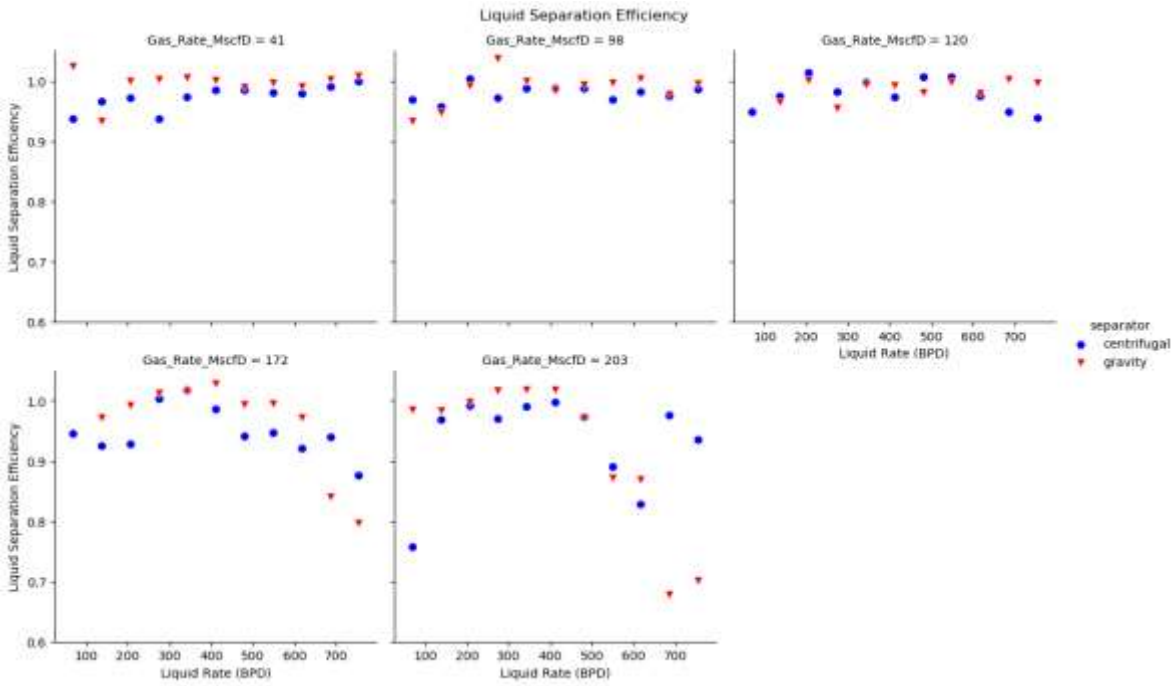

Figure 4.26. Comparison of liquid separation efficiency

Despite the similarities in the results, there is a wide difference between the efficiency of the centrifugal and gravity separator at liquid rates above 600 BPD for these two high gas rates. The efficiency of the gravity-type separator decreases rapidly for high liquid rates at 172 and 203 MscfD gas rates. It was also very difficult to control the gravity-driven separator at these high gas rates. Some of the tests were repeated multiple times before steady state measurements could be made.

4.4.1 Gas Separation Efficiency Analysis

Gas separation efficiency can be considered more important than liquid separation efficiency when it comes to the pump's performance. Gas efficiency is a measure of how efficiently the separator keeps large bubbles away from the pump. It is defined as the proportion of the outlet gas rate that is produced from the casing. However, gas efficiency analysis is limited in this study, because only the data from the high accuracy new flowmeter at the tubing return line

(ATRL) were considered. The number of collected data points on the centrifugal separator with the new flowmeter is limited. The analysis of gas separation efficiency is presented in Figure 4.27. The observation is like that of the liquid separation efficiency in Figure 4.26. The gravity-driven separator provides a lower gas separation efficiency than the centrifugal type at high gas and liquid flowrates. More tests should be run at extended liquid and gas rates to get a better understanding of the differences between the two separators.

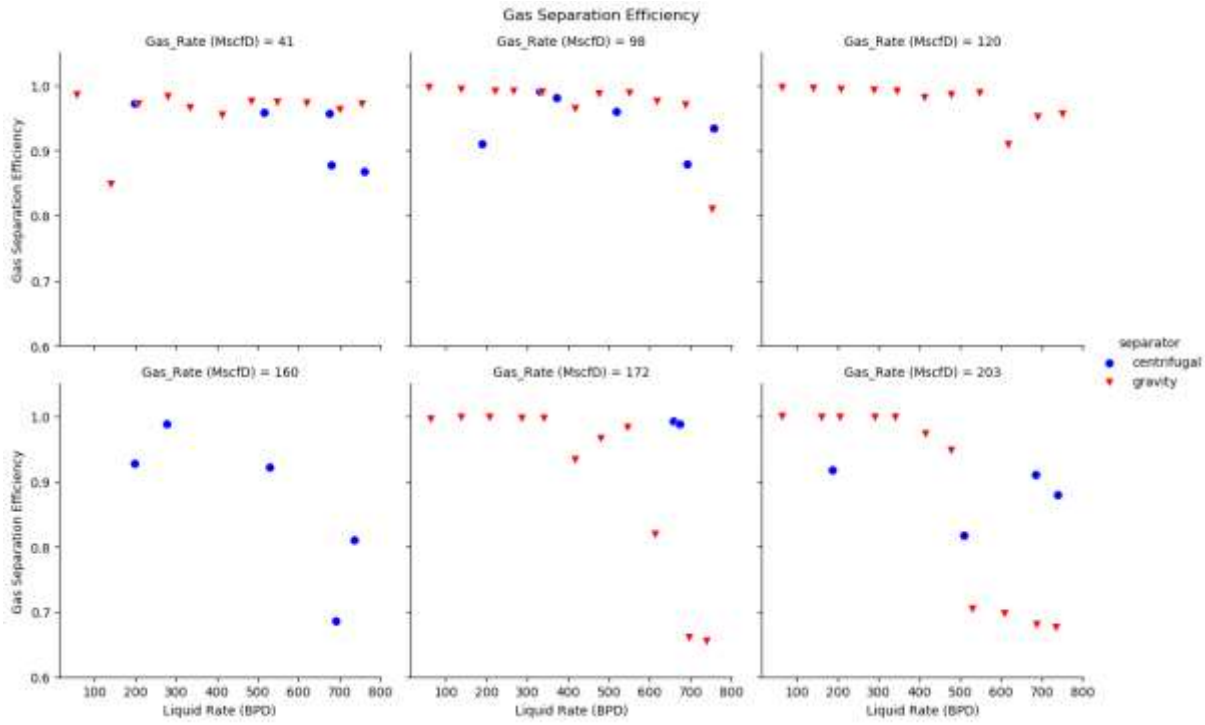

Figure 4.27. Comparison of gas separation efficiency

Figure 4.28 compares the distributions of both liquid and gas efficiencies for the two tested separators. Gravity separator has higher median values for both liquid and gas separation efficiencies. However, it is more dispersed than the centrifugal separator. The results of the centrifugal separator are more consistent than those of the gravity-type separator. This is because the centrifugal separator maintains an acceptable performance at high-end of liquid and gas flowrates, as shown earlier.

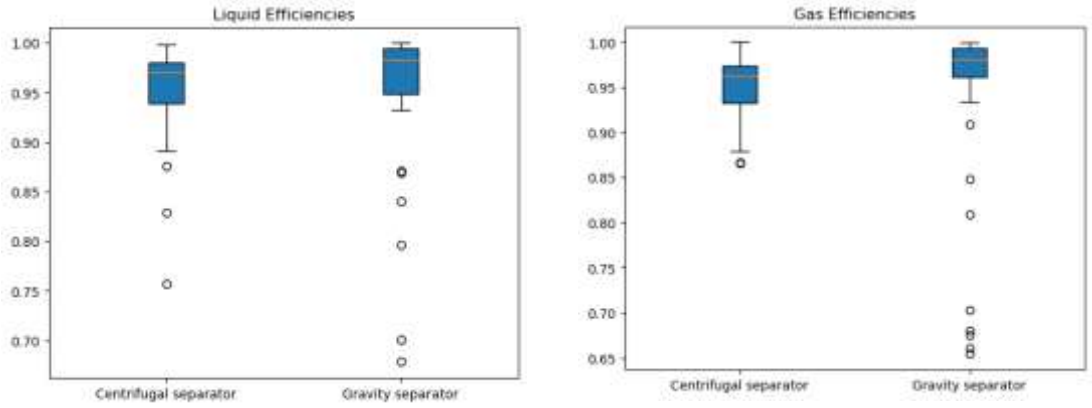

Figure 4.28. Comparison of gas and liquid efficiency distribution

Figure 4. 29 shows the comparison of outlet GOR and inlet GOR in scf/bbl. The diagonal line represent points of equal inlet and outlet GOR. All the data points lie below the diagonal line which indicates lower GOR at the outlet for every inlet GOR.

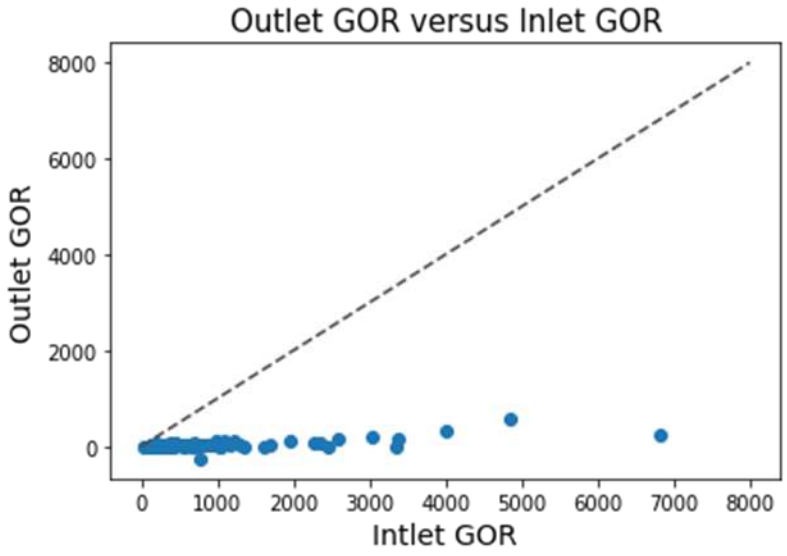

Figure 4. 29. Outlet GOR versus Inlet GOR

Figure 4. 30 shows the liquid separation efficiency for all the inlet GOR values tested. Most of the tests were conducted at low GOR and their liquid separation efficiency range from as low as 0.8 to 1.0.

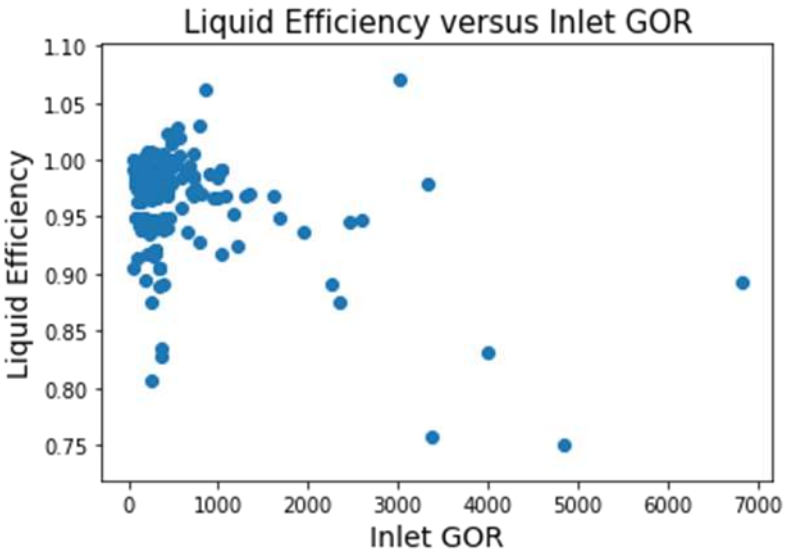

Figure 4. 30. Liquid efficiency against Inlet GOR

However, most of the tests with GOR values higher than 2000 scf/bbl have liquid separation efficiency less than 0.9. It is a safe conclusion than separation efficiency reduces as GOR values increases.

4.5 Practical Discussions

Water and air have been used as the experimental fluids in this study. The properties of both fluids differ considerably from high pressure gas and oil, encountered in field applications. The expected effects of field complications, such as changes in density and viscosity, and the effects of foaming are highlighted below:

1. Crude oil is more viscous than water. An increase in viscosity leads to more gas bubbles being trapped in the liquid phase, thereby reducing the gas separation efficiency of the separator. A centrifugal separator could potentially perform better than a gravity separator, because of the presence of additional centrifugal forces.

2. Oil is less dense than water, while air is less dense than the pressurized natural gas. The density contrast between oil and natural gas is hence lower than the contrast between water

and air. A reduction in the density contrast could cause a reduction in separation efficiency of both separators, because of the reduction in the relative motion of the two phases. On the other hand, reducing the liquid density reduces the downward velocity of the liquid phase in the casing annulus thereby giving more time for the gas phase to separate. A more detailed analysis is required to quantify the performances of the separators under these conditions.

3. Foaming is another common factor in actual field operations. It is harder for the individual phases to break free in the presence of foam. The tests of this study were conducted with no chemicals in the liquid phases, eliminating the possibility of stable foams in the casing. However, from visual observations, the liquid at the shroud of the basic gravity separator was cloudier than that of the centrifugal separator. The centrifugal forces act to break the foam bubbles in the centrifugal separator, making the gravity separator more susceptible to entraining small gas bubbles. Hence, the centrifugal separator will likely perform better than the gravity separator in presence of foam.

CHAPTER 5: CONCLUSIONS AND RECOMMENDATIONS

This study is an effort to better understand and evaluate the downhole separation technology. Two separators with different separation techniques were experimentally evaluated and compared. The tests were conducted using a large-scale experimental facility over a wide range of liquid and gas rates. Both liquid and gas flows were carefully measured at the inlet, casing outlet and tubing outlet, and used to evaluate the separators. The conclusions drawn from analyzing the results are presented in this chapter. In addition, recommendations are provided for expanding the scope of this study in future to get a better understanding of the principles of downhole separation.

5.1 Conclusions

The following conclusions summarize the main findings of this work:

1. The performances of both separators can be considered acceptable for the conducted tests, covering a range of 17 -867 bpd for liquid rate and 41-203 Mscf/d for gas rate. The separation efficiencies are generally higher than 90%.
2. Liquid separation efficiency values are highest at median liquid flowrates for all of the gas rates examined. The low and high ends of the flow rates are associated with slightly lower separation efficiency values.
3. For both separators, variation of liquid production output at the TRL reduces as liquid rate increases for the same gas rate. Also, variation decreases as gas rate increases at the same liquid flowrate. This variation is a result of fluctuation in casing liquid level and implies an unstable flow. Hence, flow instability is associated with low liquid and gas rates.

4. The separators have similar values of separation efficiency at similar conditions. It is hard to conclude which separator has a better separation efficiency. The only difference is at the high-end of liquid and gas rates, where both separators show declines in efficiency. However, the drop in the efficiency of the gravity separator is much sharper.
5. Visual observations indicate that larger bubbles are drawn into the shroud for the basic gravity separator, while these bubbles are smaller for the centrifugal separator. This implies that the centrifugal separator is better at sending larger bubbles up the casing and away from the tubing.
6. Comparison of the coefficients of variation for the two separators indicates that the centrifugal separator is more stable. It delivers a steadier liquid production at the tubing outlet than the basic gravity separator.
7. Liquid level in the annulus should be maintained at a sufficient distance from the casing head to prevent liquid carryover into the casing return line. This may otherwise result in a reduction in liquid separation efficiency.
8. Gas separation efficiencies of the two separators were also compared for a limited number of tests. Similarly, both separators show high gas separation efficiencies with declines in high gas and liquid rates. The decline is sharper for the gravity separator compared to the centrifugal one.

5.2 Recommendations

1. The study may be extended to higher liquid rates to examine the performance of the separators at ranges more compatible with the well using ESP's. It is important to evaluate the separators and check for the possibility of trends in the performance data.

2. The length of the separator shroud could be varied to examine its effect on separation performance. Similarly, the geometry of the separator, and particularly, the length of the spiral section may be optimized.
3. The flow pattern of the mixture upstream of the separator could be recorded and the effect of flow pattern changes on separation efficiency could be examined in future studies.
4. The effect of separator length on separation efficiency could be examined in the future.
5. Tests may be conducted at higher pressures to evaluate the separation efficiency at higher gas densities, closer to the field conditions.
6. Further analysis of the separators could also be performed using computational fluid dynamics (CFD).

Appendix

Component	Gas	Gas Condensate	Volatile Oil	Black Oil
N_2	0.3	0.71	1.67	0.67
CO_2	1.1	8.65	2.18	2.11
C_1	90.0	70.86	60.51	34.93
C_2	4.9	8.53	7.52	7.00
C_3	1.9	4.95	4.74	7.82
C_4 $(i+n)$	1.1	2.00	4.12	5.48
C_5 $(i+n)$	0.4	0.81	2.97	3.80
C_6 $(i+n)$	6+: 0.3	0.46	1.99	3.04
C_7		0.61	2.45	4.39
C_8		0.71	2.41	4.71
C_9		0.39	1.69	3.21
C_{10}		0.28	1.42	1.79
C_{11}		0.20	1.02	1.72
C_{12}		0.15	12+: 5.31	1.74
C_{13}		0.11		1.74
C_{14}		0.10		1.35
C_{15}		0.07		1.34
C_{16}		0.05		1.06
C_{17}		17+: 0.37		1.02
C_{18}				1.00
C_{19}				0.90
C_{20}				20+: 9.18

Figure A. 1: Typical molar compositions of petroleum fluids (from Pedersen et al., 1989)

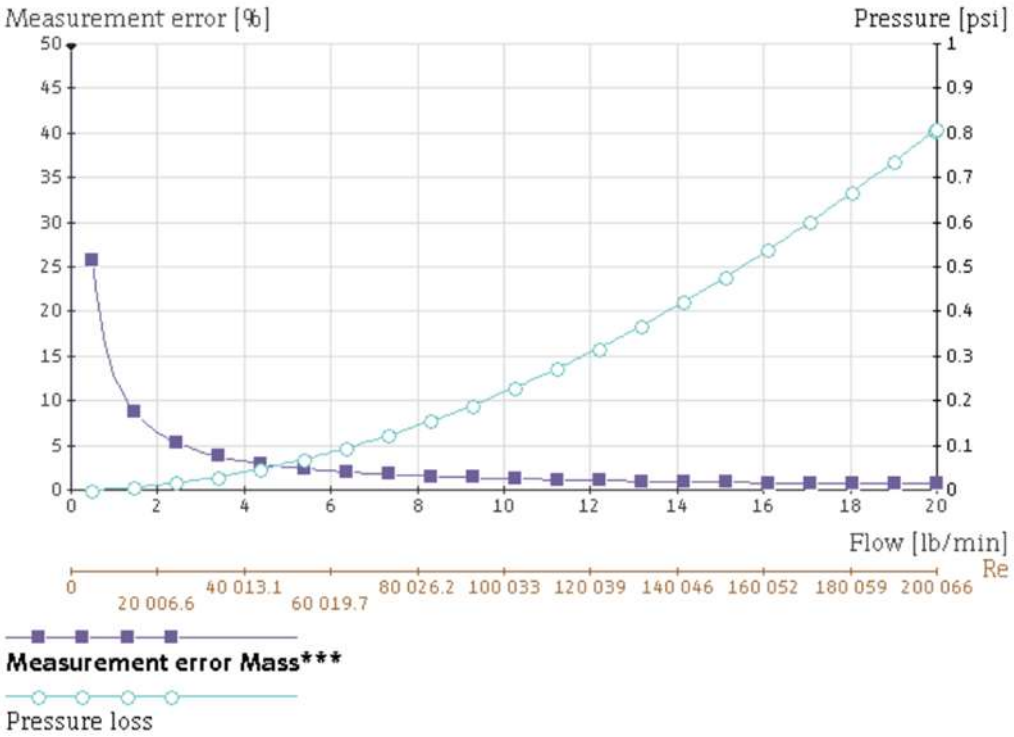

Figure A. 2: Error chart for 2'' Coriolis flowmeter

References

Sharma, A. (2019). Experimental evaluation of a centrifugal packer-type downhole separator. In Shareok (Vol. 4, Issue 1). https://hdl.handle.net/11244/323223

Bohorquez, R., Ananaba, V., Alabi, O., Podio, A. L., Lisigurski, O., & Guzman, M. (2009). Laboratory testing of downhole gas separators. *SPE Production and Operations*, *24*(4), 499–509. https://doi.org/10.2118/109532-PA

Lopez, J., Pereyra, E., & Sarica, C. (2019). An experimental investigation of dynamic behavior of gravity-driven downhole separators. *Proceedings - SPE Annual Technical Conference and Exhibition*, *2019-Septe*(1996). https://doi.org/10.2118/196197-ms

McCoy, J. M., Patterson, J., & Podio, A. L. (2007). Downhole gas separators - A laboratory and field study. *Journal of Canadian Petroleum Technology*, *46*(5), 48–54. https://doi.org/10.2118/07-05-05

McCoy, J. N., Patterson, J., & Podio, A. L. (2005). A laboratory study with field data of downhole gas separators. *Canadian International Petroleum Conference 2005, CIPC 2005, June 2005*, 9–12.

McCoy, J. N., Podio, A. L., Rowlan, O. L., & Becker, D. (2015). Evaluation and performance of packer-type downhole gas separators. *SPE Production and Operations*, *30*(3), 236–242. https://doi.org/10.2118/164510-PA

Torre, A. J., Schmidt, Z., Blais, R. N., Doty, D. R., & Brill, J. P. (1987). Casing Heading in Flowing Oil Wells. *SPE Production Engineering*, *2*(4), 297–304. https://doi.org/10.2118/13801-PA

Kobylinski, L. S., Taylor, F. T., & Brienan, J. W. (1985). Development and Field Test Results of an Efficient Downhole Centrifugal Gas Separator. *JPT, Journal of Petroleum Technology*, *37*(8), 1295–1304. https://doi.org/10.2118/11743-pa

Ibarra, J., Pardo, R., Vega, L., & Carios, E. (2013). Experimental study of a poor boy downhole gas separator under continuous gas-liquid flow. *Society of Petroleum Engineers - 2013 SPE Artificial Lift Conference - Americas: Artificial Lift: Where Do We Go From Here*, *1996*, 206–216.

Mccoy, J. N., Rowlan, O. L., Company, D. B. E., & Podio, A. L. (2013). *Optimizing Downhole Packer-Type Separators Packer-type Separators*.

Downhole Diverter Gas Separator Jim McCoy, O. Lynn Rowlan, Dieter Becker of Echometer Company. A. L. Podio, University of Texas. (2013). 1–19.

Alabi, O., & Podio, A. L. (2009). Laboratory testing of downhole gas separators in inclined wellbore configurations. *Proceedings - SPE Annual Technical Conference and Exhibition*, *6*(July 2007), 4098–4112. https://doi.org/10.2118/124986-ms

Sharma, A., Iradukunda, P., Karami, H., McCoy, J. N., Podio, A. L., & Teodoriu, C. (2020). Experimental evaluation of a prototype centrifugal packer-type downhole separator. *Society of Petroleum Engineers - SPE Artificial Lift Conference and Exhibition - Americas 2020, ALCE 2020*. https://doi.org/10.2118/201147-ms

Mccoy, J. N., Company, E., Rowlan, O. L., Company, E., Ellithorp, B., & Company, E. (2017). *Gas separator selection and performance*. 1–12.

Lopez, J., Pereyra, E., & Sarica, C. (2020). An experimental investigation of a highly deviated shroud type downhole separators. *Society of Petroleum Engineers - SPE Artificial Lift Conference and Exhibition - Americas 2020, ALCE 2020*. https://doi.org/10.2118/201127-ms

Olubode et. al. (2022). Experimental analysis of centrifugal downhole separators in boosting artificial lift performance.